Energy Advances

ROYAL SOCIETY OF CHEMISTRY

REVIEW ARTICLE

View Article Online
View Journal | View Issue

Check for updates

Cite this: *Energy Adv.*, 2023, 2, 252

Metal–organic framework-derived single atom catalysts for electrocatalytic reduction of carbon dioxide to C1 products

Xu Han,†[a] Ting Zhang†[a] and Jordi Arbiol *[ab]

Received 19th October 2022,
Accepted 30th November 2022

DOI: 10.1039/d2ya00284a

rsc.li/energy-advances

Electrochemical carbon dioxide reduction reaction (eCO_2 RR) is an efficient strategy to relieve global environmental and energy issues by converting excess CO_2 from the atmosphere to value-added products. Single-atom catalysts (SACs) derived from metal–organic frameworks (MOF), which feature unique active sites and adjustable structures, are emerging as extraordinary materials for eCO_2 RR. By modulating the MOF precursors and their fabrication strategy, MOF-derived SACs with specific-site coordination configuration have been recently designed for the conversion of CO_2 to targeted products. In the first part of this review, MOF synthesis routes to afford well-dispersed SACs along with the respective synthesis strategy have been systematically reviewed, and typical examples for each strategy have been discussed. Compared with traditional M-N_4 active sites, SACs with regulated coordination structures have been rapidly developed for eCO_2 RR. Secondly, the relationship between regulation of the coordination environment of the central metal atoms, including asymmetrical M-N_x sites, heteroatom doped M-N_x sites, and dual-metal active sites (M–M sites), and their respective catalytic performance has been systematically discussed. Finally, the challenges and future research directions for the application of SACs derived from MOFs for eCO_2 RR have been proposed.

Open Access Article. Published on 30 de novembre 2022. Downloaded on 27/1/2026 21:08:31.
This article is licensed under a Creative Commons Attribution 3.0 Unported Licence.

1. Introduction

A high concentration of carbon dioxide (CO_2) in the atmosphere caused by burning fossil fuels since the industrial revolution has gradually triggered increasing environmental issues, such as global warming, extreme weather, species extinction and rising of the sea levels.[1–3] To reduce the CO_2 concentration in the atmosphere, significant efforts have been undertaken to maintain the carbon cycle, which largely relies on accelerating the development of a large number of technologies. Two main approaches have been recently proposed to address the above issues: (1) the physical capture and storage of CO_2 and (2) the chemical conversion of CO_2 into useful chemicals.[4,5] Compared to the former, converting CO_2 to renewable chemicals/fuels is an attractive and effective method, because fossil fuels are still the main source for providing energy, and therefore conversion of CO_2 can not only mitigate CO_2 emission but also alleviate the energy shortage (Fig. 1).[4,6,7] Over the past few decades, CO_2 conversion technologies have included photochemical,[8] electrochemical[9] and biological[10] related processes. Among them, the electrochemical reduction of CO_2 (eCO_2 RR) driven by renewable power (like wind and solar) to produce higher-value chemical products is especially desirable in terms of energy efficiency and cost because of (1) controllable electrode potentials and ambient reaction temperatures as well as pressures; (2) recycled electrolytes, minimizing overall chemical consumption; (3) reduced

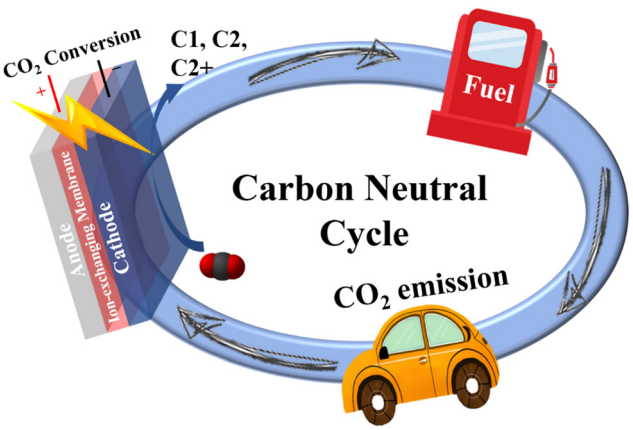

Fig. 1 The schematic illustration of a carbon neutral cycle based on electrochemical CO_2 reduction reaction.

[a] *Catalan Institute of Nanoscience and Nanotechnology (ICN2), CSIC and BIST, Campus UAB, Bellaterra, Barcelona, 08193, Catalonia, Spain. E-mail: arbiol@icrea.cat*
[b] *ICREA, Pg. Lluís Companys 23, Barcelona, 08010, Catalonia, Spain*
† Equal contribution.

© 2023 The Author(s). Published by the Royal Society of Chemistry

Open Access Article. Published on 30 de novembre 2022. Downloaded on 27/1/2026 21:08:31. This article is licensed under a Creative Commons Attribution 3.0 Unported Licence.

generation of new CO_2 sources due to electricity as the driver; and (4) easy scale-up applications.[6,11,12] Therefore, eCO_2 RR provides a promising way for generating chemical energy, which can be regarded as a form of renewable energy storage.

The eCO_2 RR process is divided into three main steps, including the adsorption of CO_2 on active sites for CO_2* formation, electron/proton transfer for cleaving the C=O bond and producing different intermediates, and desorption and diffusion of products from active sites.[13–18] Until now, eCO_2 RR has faced many problems due to the thermodynamic stability and chemical inertness of CO_2 as a reactant (the dissociation energy of a C=O bond is about 806 kJ mol^{-1}).[19] The first activation step of CO_2 to form CO_2^{*-}, occurring at −1.9 V *versus* standard hydrogen electrode (SHE) (Table 1), leads to a high CO_2 activation barrier and insufficient efficiencies.[20,21] In addition, the thermodynamical potentials for producing different products are very close accompanied with the hydrogen evolution reaction (HER, Table 1), resulting in an inevitable effect on the desirable product selectivity.[22,23] Based on the number of carbon atoms, the eCO_2 RR products are classified into the following categories: C1 products, including carbon monoxide (CO), formate/formic acid (HCOOH), methanol (CH_3OH) and methane (CH_4); C2 products, including ethylene (C_2H_4), ethanol (C_2H_5OH) and acetate (CH_3COOH); C3 products such as propylene (C_3H_6) and *n*-propanol (C_3H_7OH); and long-chain products.[17] Although significant progress has been made in the eCO_2 RR process, it is still limited by the lack of high-efficient electrocatalysts, showing a low energy efficiency and activity as well as poor selectivity because of the complex product distributions. Designing eCO_2 RR electrocatalysts with high activity and selectivity for a particular product is thus highly desirable to speed up the sluggish eCO_2 RR and solve the above problems.

Single-atom catalysts (SACs) with atomically dispersed catalytic sites, which are anchored on a specific support, were first reported by Zhang and co-workers in 2011.[24–26] Due to their unique electronic and geometric structures, SACs inherit the advantages of both heterogeneous and homogeneous catalysts, and have recently emerged as an up-to-date frontier in materials science. They have shown great potential in energy-related catalysis owing to the (1) maximization of the percentage of metal atoms as active sites; (2) increase of the effective active site density; (3) regulation of the central metal atoms and coordination environments; and (4) adjustment of the electronic structure.[27–34] Benefiting from the simple and precise single metal-based active sites, their catalytic performance can be easily regulated, which helps to overcome the high activation barriers and the sluggish kinetics in eCO_2 RR, and therefore SACs have recently been developed in eCO_2 RR with excellent selectivity and activity, opening a way to improve the CO_2 conversion. In addition, their simplicity has allowed one to deeply and comprehensively understand the relationship between the structures and their catalytic performance.[35–39] Fig. 2 summarizes different reported metal centers in SACs for eCO_2 RR, which include three types based on the nature of the metal centers: (1) transition metals (Co,[40,41] Fe,[42,43] Ni,[44,45] Cu,[46,47] Zn[48,49] and Mo[50,51]), (2) noble metals (Pd,[52,53] Au[54] and Ag[55,56]) and (3) p-block elements (Sn[57–59] and Bi[60]).

Although there have been some significant efforts in the design of SACs for eCO_2 RR, due to their high surface energies when dispersing catalysts at the atomic level, the fabrication of SACs still suffers from low porosity structures and low metal loading (<1.0 wt%), as well as the tendency for metal aggregation.[61–64] As a result, exploring a controlled strategy to construct SACs with suitable supports to bear porous structures, uniform atomic sites, high metal content and strong coordination environments is of critical importance to avoid agglomeration during preparation and subsequent reaction efficiency improvement.

Several synthetic methodologies have been developed and explored in order to obtain SACs. The main ones have been coprecipitation,[65] impregnation,[66] atomic layer deposition[67] and the use of metal–organic frameworks (MOFs) as templates.[60,68–74] Among them, the use of MOFs as templates, with regular frame structures and uniform pores constructed by coordinating bridging organic ligands and metal centers, has been considered as one of the most promising approaches for preparing high quality SACs.[61–64,72,75] Owing to the spatial separation effect of MOFs, single metal sites with uniform dispersion can be accommodated into their metal nodes, organic ligands or pores at different locations.[61,63,64,76] For example, ZIF-8 as the "star" MOF, with a pore diameter of 3.4 Å, which can be used to prepare nanoporous carbon materials with an unexpectedly high surface area by direct pyrolysis,[77] has been widely used as a template to prepare a large number of SACs, by efficiently encapsulating different metal atom species.[37,78,79] After pyrolysis, the single atom (SA) embedded into the carbon support derived from ZIF-8 is generated *via* coordination bonds with surrounding chelating atoms, such as N, which in this case come from 2-methylimidazole. Functional UiO-66-NH_2 can also coordinate and confine the metal ions in the skeletons through uncoordinated amino groups, further inhibiting the migration of metal species.[80] Followed by a thermal treatment, different SACs have been also obtained by using UiO-66-NH_2 as a MOF template. In most cases, compared to other SAC preparation approaches, the SACs derived from MOFs have many merits: (1) due to pyrolysis at a high temperature, such SACs can be used in harsher conditions with long-term stability compared to those obtained by other conventional synthetic

Table 1 Standard potentials of possible reactions occurring in the eCO_2 RR (V *vs.* SHE)

Half-electrochemical reactions	Standard potential (V *vs.* SHE)
$2H^+ + 2e^- \rightarrow H_2$	−0.42
$CO_2 + 2H^+ + 2e^- \rightarrow CO + H_2O$	−0.52
$CO_2 + 2H^+ + 2e^- \rightarrow HCOOH$	−0.61
$CO_2 + 4H^+ + 4e^- \rightarrow HCHO + H_2O$	−0.51
$CO_2 + 6H^+ + 6e^- \rightarrow CH_3OH + H_2O$	−0.38
$CO_2 + 8H^+ + 8e^- \rightarrow CH_4 + 2H_2O$	−0.24
$2CO_2 + 12H^+ + 12e^- \rightarrow C_2H_4 + 4H_2O$	−0.34
$2CO_2 + 12H^+ + 12e^- \rightarrow C_2H_5OH + 3H_2O$	−0.33
$CO_2 + e^- \rightarrow CO_2^{*-}$	−1.90

© 2023 The Author(s). Published by the Royal Society of Chemistry

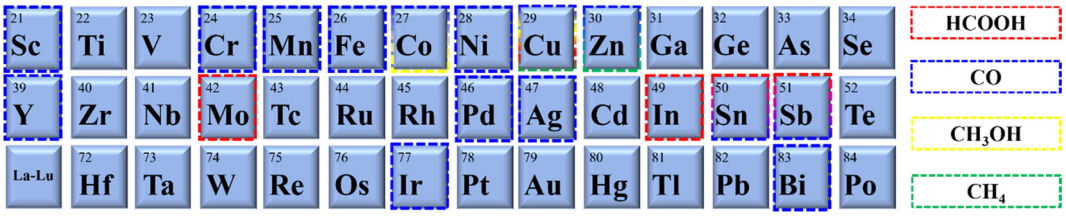

Fig. 2 The reported products on SACs with different metal centers for eCO_2 RR.

Open Access Article. Published on 30 de novembre 2022. Downloaded on 27/1/2026 21:08:31.
This article is licensed under a Creative Commons Attribution 3.0 Unported Licence.

methods; (2) such SACs have a large surface area and high porosity inherited from parent MOFs, which could facilitate electron and mass transport as well as increase the accessibility to active SA sites, leading to an unexpected eCO_2 RR performance.[28,61,75,81,82] Therefore, tremendous efforts have been devoted for optimizing MOF-derived SACs. In Fig. 3, a brief history of the development and the latest progress of MOF derived SACs for eCO_2 RR is presented. In addition, MOF-derived SACs have been divided into two categories according to their synthetic approaches.

1.1 Formation of SACs by direct pyrolysis of MOFs

MOFs are composed of various metal nodes and organic ligands; thus, the atomically dispersed metal species can be derived from the metal nodes in the frameworks after pyrolysis. In this strategy, suitable MOFs have been chosen to form the targeted SACs after thermal, acid-etching or activation treatments. For instance, Jiang *et al.* prepared a Zn SAC derived from ZIF-8 with an ultrahigh Zn loading mass (11.3 wt%).[83] However, during the direct preparation, metal nanoparticles are also generated when using this method, accompanied by the formation of SACs. In this way, a post-acid treatment is usually used to effectively remove the metal particles, leaving the atomically dispersed metal sites anchored on the carbon-based substrates.[84–86] For instance, a highly dispersed manganese (Mn) SAC was reported by Yang *et al.* by directly pyrolyzing Mn-based MOFs.[85] The former procedure allowed the removal of the residual MnO particles created by applying an acid-etching process: in parallel, the same process generated a porous structure. Despite substantial achievements made in this strategy, the universality of this approach is still limited by the tedious acid treatment or activation process, which not only increases the synthetic complexity, but also leads to a low metal loading.

1.2 Formation of SACs by pyrolysis of MOFs with the second metal addition

In this strategy, additional targeted metals are introduced into the metal nodes or pores of MOF precursors for forming SACs after pyrolysis. Up to now, among many MOF precursors, Zn-based MOFs with nitrogen-rich organic linkers are the ones preferred. On the one hand, it is feasible to form the metal–nitrogen coordination interaction after pyrolysis, which can stabilize the SACs. On the other hand, because of the relatively low boiling point of Zn (906 °C), most of the Zn metal atoms are evaporated as a self-sacrificial metal during pyrolysis, which can avoid the formation of excess metal hybrids, leaving the targeted metals atomically dispersed on the porous carbon.[68,87–90] For example, second metal ions (like Co^{2+},[87,91,92] Ni^{2+},[68,93] Fe^{3+},[69,94] *etc.*) have been successfully implanted into Zn-based MOFs with homogeneous dispersion in metal nodes or pores, resulting in a

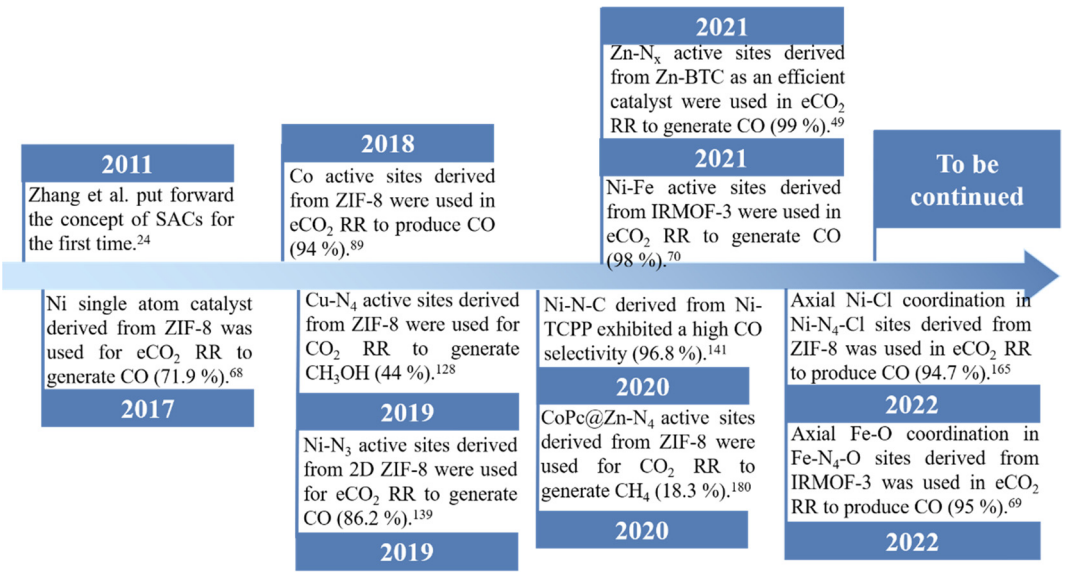

Fig. 3 A brief history of the development of SACs derived from MOFs.

© 2023 The Author(s). Published by the Royal Society of Chemistry

Open Access Article. Published on 30 de novembre 2022. Downloaded on 27/1/2026 21:08:31.
This article is licensed under a Creative Commons Attribution 3.0 Unported Licence.

much longer spatial distance between each other. By this means, single-atom Co, Ni, and Fe sites anchored on a N-doped carbon support have been successfully synthesized by pyrolysis of pre-designed bimetallic MOFs.

The utilization of SACs in eCO_2 RR has made progress in recent years, owing to the use of MOFs as templates to synthesize these SACs, opening a new chapter for eCO_2 RR. Although many reviews on SACs for eCO_2 RR have been reported recently, the study of eCO_2 RR catalyzed by MOF-derived SACs influenced by the coordinated environment is still in its infancy. Therefore, this review will not only focus on the development of SACs derived from MOFs, but also give a discussion of the relationship between the coordination environments of MOF-derived SACs and their catalytic performance. Due to the simple separated active sites in SACs, the carbon–carbon coupling is difficult. Therefore, C1 products are the preferred ones over most SACs derived from MOFs, instead of longer hydrocarbon chains. In this way, we will mainly focus on C1 products, including CO, HCOOH, CH_3OH and CH_4. In addition, some challenges in such field are also provided at the end of the present work. This review is intended to provide an overview for the future design of MOF-derived SACs for eCO_2 RR *via* the accurate elucidation of their structure–activity relationship.

2. Fundamentals of the eCO_2 RR

ECO_2 RR occurs on the cathode surface and involves a multi-electron/proton transfer process. The main C1 products, CO, HCOOH, CH_3OH and CH_4, can be obtained by transferring 2, 4, 6, and 8 electrons, respectively, with the consequent reduction of CO_2 based on the applied potential. The possible pathways for the main C1 products are given below. CO_2 reduction to CO and HCOOH can start with a one proton/electron transfer to a CO_2 molecule followed by the stabilization of COOH* and OCHO* intermediates.[36,95,96] Subsequently, for CO generation, COOH* is transformed to CO* through a dehydrogenation reaction, and then, the CO* desorbs from the catalysts' surfaces, forming the final CO product.[19,97] In addition, *CO can be further reduced to generate multi-electron products if it binds to the catalyst surface strongly. With a succession of proton-coupled electron transfers, CH_3OH and CH_4 can be generated.[2,98] It is worth mentioning that the energy barriers to produce CH_3OH are high, making CH_3OH generation rather difficult.[96] In the case of HCOOH generation, the OCHO* intermediates desorb from the metal surface to form HCOOH.

2.1 CO_2-to-CO pathway

Among all the eCO_2 RR products, from a commercial point of view, CO is considered as the most attractive targeted product because it can be produced with a high faradaic efficiency (FE) exceeding the hitherto reported value of 90% and only requires a simple two-electron/proton transfer pathway with low energy barriers.[19,99–103] Meanwhile, CO and H_2, as syngas, can be utilized to produce various commodity chemicals in industry *via* the Fischer–Tropsch process.[17,104] So far, the majority of reported SACs have shown high catalytic activity towards CO_2-to-CO reaction, which is comparable to that of noble metal catalysts, such as Au and Ag. The proposed mechanisms for CO_2-to-CO reaction on SACs are often divided into two categories: (1) the pathway of CO_2 RR to CO *via* a carboxyl (*COOH) intermediate and (2) a proton decoupled electron transfer related mechanism (Fig. 4).[48,105,106] These proposed reaction mechanisms merely represent the reaction pathway for a specific catalyst and condition.

The first conversion mechanism consisting of the pathway of CO_2 RR to CO *via* a carboxyl (*COOH) intermediate is proposed to occur in three steps:

(i) $CO_2(g) + e^- + H^+ \rightarrow$ *COOH;

(ii) *COOH + e^- + $H^+ \rightarrow$ *CO + H_2O;

(iii) *CO $\rightarrow$ CO + *;

where * indicates that the molecule is adsorbed on the surface of the catalysts.[107,108] *COOH forms *via* a concerted protonation and electron transfer. Then, the *COOH intermediate converts to *CO *via* further proton–electron transfer. Finally, *CO dissociates from the active sites to generate CO. For instance, the formation of the Fe-N_4-COOH intermediate from CO_2 *via* a concerted protonation and electron transfer process has been proposed by Chen *et al.* on FeN_4 sites.[109]

The second mechanism, which consists of proton decoupled electron transfer, includes the following steps:

(i) formation of an adsorbed $CO_2^{\bullet -}$ *via* one-electron transfer;

(ii) a protonation process of $CO_2^{\bullet -}$ to form *COOH;

(iii) *COOH + e^- + $H^+ \rightarrow$ *CO + H_2O;

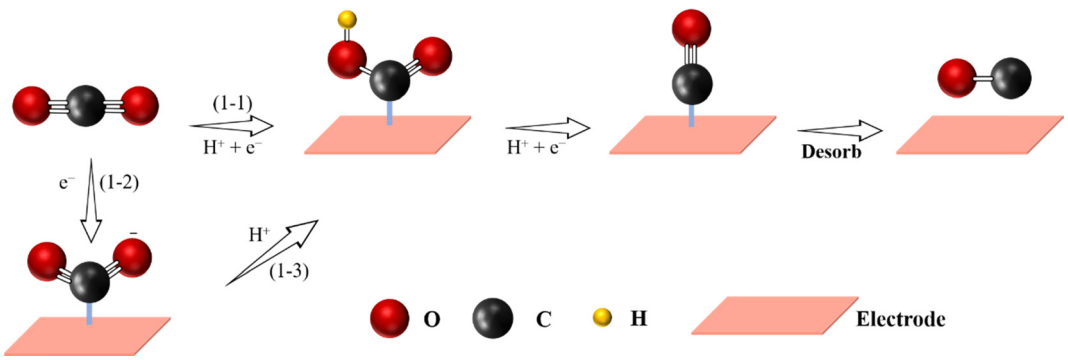

Fig. 4 Proposed reaction pathway for electrochemical CO_2-to-CO reaction (C atoms: gray; O atoms: red; H atoms: yellow).

Open Access Article. Published on 30 de novembre 2022. Downloaded on 27/1/2026 21:08:31.
This article is licensed under a Creative Commons Attribution 3.0 Unported Licence.

(iv) *CO → CO + *;

where * indicates that the molecule is adsorbed on the surface of the catalysts.[110,111] Such a mechanism was proposed on a Fe-based SAC, consisting of a homogeneous molecular catalyst with metal–N macrocyclic complexes. Despite the above proposed mechanisms, the development and improvement of advanced characterization methods, especially operando spectroscopic techniques, to investigate in more detail the mechanisms of eCO_2 RR, are still needed.

2.2 CO_2-to-HCOOH pathway

As an essential energy-dense carrier for many industrial processes,[112,113] formic acid/formate ($HCOOH/HCOO^-$) ($HCOO^-$ exists at pH > 4.1, while HCOOH exists at pH < 4.1) can be sustainably produced from eCO_2 RR,[114–116] which is also a two-electron process consisting of 3 steps[37,100] (Fig. 5):

(i) $CO_2 + H^+ + e^- \rightarrow$ *OCHO;

(ii) *OCHO + $H^+ + e^- \rightarrow$ *HCOOH;

(iii) *HCOOH → * + HCOOH.

Similarly, the first conversion mechanism step for the formation of HCOOH in eCO_2 RR consists of the generation of $*CO_2^{\bullet-}$ *via* one-electron transfer. Secondly, the formation of the *OCHO intermediate involves a protonation process. The same intermediate (*OCHO) through a proton-coupled electron transfer (PCET) step can be formed after direct gaseous CO_2 conversion. An alternative process is the generation of *OCHO through the attack and insertion of the CO_2 molecule on *H species. Finally, through another PCET step, the *OCHO intermediate is converted to HCOOH or $HCOO^-$.[117] Generally, Sn,[118] Pb,[117] Bi,[119] In,[120] Pd,[100] and other metal-free catalysts[121] possess high selectivity towards HCOOH or $HCOO^-$ formation. In a similar way to the bulk catalysts, in some cases, SACs with the above metal centers also showed HCOOH selectivity in eCO_2 RR. For instance, single In active sites were supported on a MOF-derived N-doped carbon matrix and used to trigger the CO_2-to-HCOOH reaction.[122] In comparison to the N–C sample, In-based SACs exhibited a higher FE (80%) towards HCOOH under a low applied potential of −0.80 V *vs.* RHE. In addition, by replacing the In metal centers by Sn,[123] these Sn-based SACs also exhibited good selectivity (62%) towards HCOOH. In this way, the strong electronic interaction between Sn single-atoms and the N-doped carbon materials could increase the bonding strength of the $CO_2^{\bullet-}$ intermediate, thereby promoting the conversion of CO_2 to HCOOH.

2.3 CO_2-to-CH_3OH pathway

As a basic organic chemical raw material, methanol has been widely used in many fields, including the production of fine chemicals, plastics or medicines.[124] In addition, due to its high energy density (4.8 kW h L^{-1}), methanol is considered as a promising fuel.[95] Nowadays, the most common method for CH_3OH formation is mixing CO and H_2 under high temperature (250–300 °C) and pressure (3.5–10 MPa).[37,95] Unfortunately, such a method usually requires high-security equipment. The eCO_2-to-CH_3OH process provides an alternative way to produce CH_3OH under moderate conditions. Compared to CO-to-HCOOH reaction, the eCO_2-to-CH_3OH reaction is a more complex process involving 6-electron transfer: $CO_2 + 6H^+ + 6e^- \rightarrow CH_3OH + 2H_2O$, making the kinetics of the reduction reaction slow, because it needs a high energy barrier to produce $*CH_2OH$ or $*CH_3O$ intermediates in the reaction, and therefore there is still a great challenge for large-scale production of CH_3OH at industry levels (Fig. 6).[2,125] Nevertheless, some interesting examples have been studied in order to materialize this reaction. For example, a CoN_4/graphene catalyst was simulated, revealing the best way to produce CH_3OH by following the next steps: CO_2 (g) → COOH* → CO* → CHO* → CH_2O* → $*OCH_3$ → CH_3OH, where the energy barrier for reducing CHO* to CH_2O* was 0.53 eV, being the speed determining step.[126] Following this idea, Wu *et al.* immobilized a cobalt-based molecular catalyst with CoN_4 active sites on carbon nanotubes showing a CH_3OH selectivity of 40%.[127] Through the above-mentioned mechanism, it is well established that *CO is an important intermediate for the formation of CH_3OH. If the adsorption energy of *CO on the catalyst's surface is high enough, the reaction further proceeds by following multiple PCET steps to generate CH_3OH. Although many efforts have been devoted to fabricate SACs for the generation of CH_3OH, the obtained activity and selectivity are still insufficient. Yang *et al.* could improve the selectivity ($FE_{methanol}$ = 44%) by designing Cu-based SACs coated on carbon nanofibers, which is a great advancement but still not sufficient for large scale industrial production.[128] Therefore, understanding the structural characteristics for designing efficient SACs for CH_3OH production is still at the early stage,

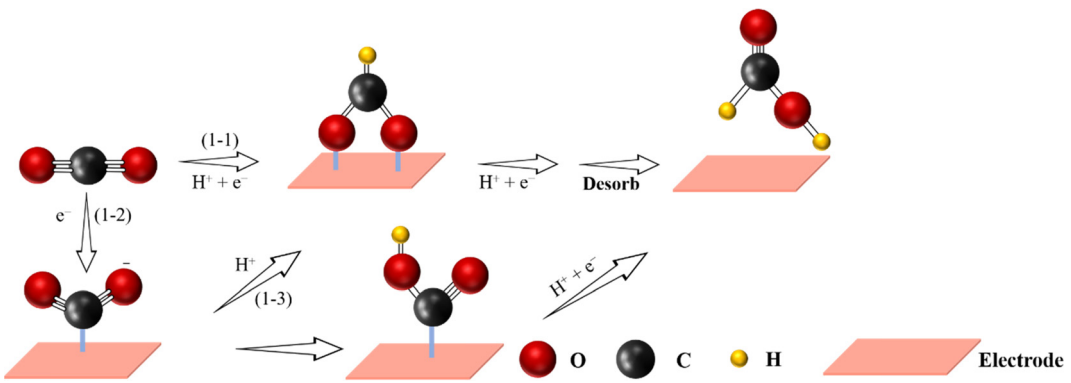

Fig. 5 Proposed reaction pathway for the electrochemical CO_2-to-HCOOH reaction (C atoms: gray; O atoms: red; H atoms: yellow).

© 2023 The Author(s). Published by the Royal Society of Chemistry

Open Access Article. Published on 30 de novembre 2022. Downloaded on 27/1/2026 21:08:31.
This article is licensed under a Creative Commons Attribution 3.0 Unported Licence.

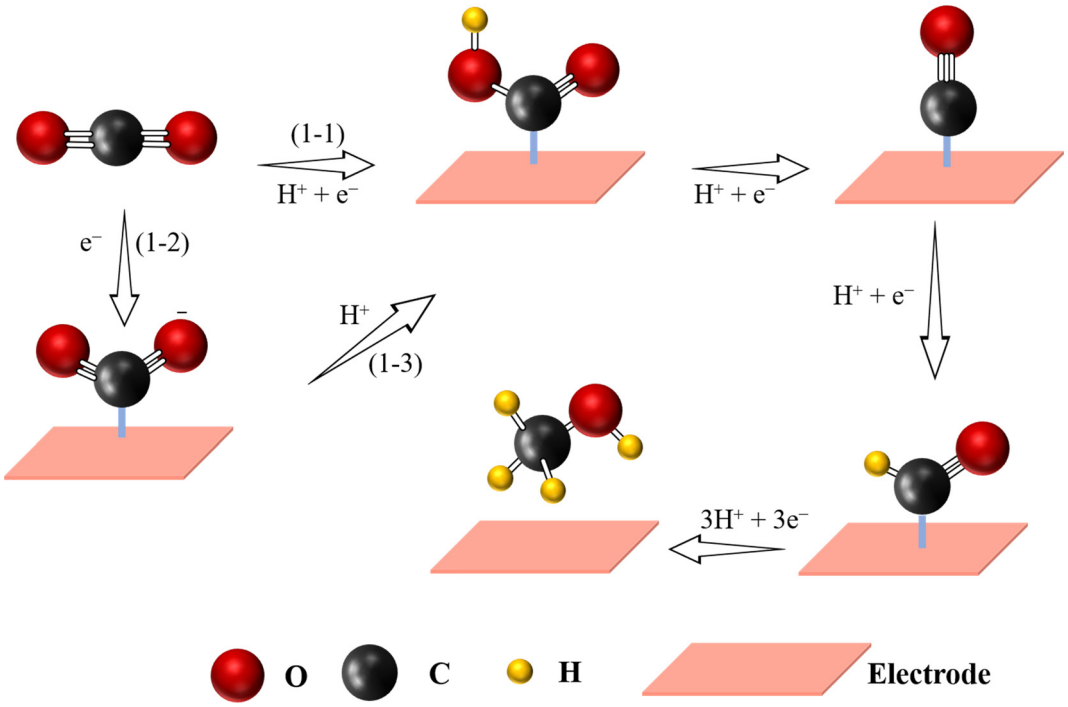

Fig. 6 Proposed reaction pathway for the electrochemical CO_2-to-CH_3OH reaction (C atoms: gray; O atoms: red; H atoms: yellow).

mainly relying on Cu-based SACs, because generation of CH_3OH (*CH_2OH and *CH_3O) presents very high energy barriers and thus its production remains a big challenge.

2.4 CO_2-to-CH_4 pathway

Methane, widely found in natural gas, is considered as a high-quality gas fuel due to the high gravimetric energy density (13.9 kW h kg^{-1}), and it can be further utilized as an energy carrier to replace traditional fossil fuels.[37,95,124] However, the electrochemical CO_2-to-CH_4 process is more difficult as it requires the transfer of 8 electrons and 8 protons: $CO_2 + 8H^+ + 8e^- \rightarrow CH_4 + 2H_2O$ (Fig. 7). Therefore, the activity and selectivity for the formation of CH_4 are low.[2] Moreover, the presence of the *CO intermediate on the active sites is important in order to

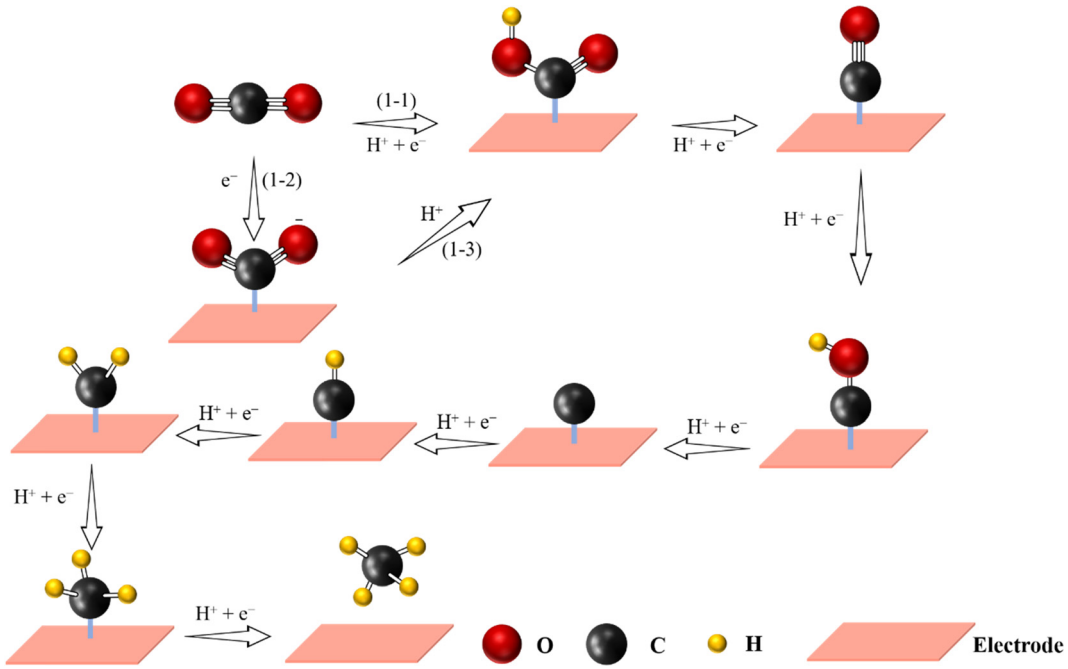

Fig. 7 Proposed reaction pathway for electrochemical CO_2-to-CH_4 reaction (C atoms: gray; O atoms: red; H atoms: yellow).

Open Access Article. Published on 30 de novembre 2022. Downloaded on 27/1/2026 21:08:31.
This article is licensed under a Creative Commons Attribution 3.0 Unported Licence.

generate CH_4. Furthermore, the generation of *CHO intermediates *via* protonation of *CO needs to overcome a large energy barrier, thus leading to a higher negative potential. As illustrated above, following the formation of *CHO, an adsorbed carbon species (*C) is formed. After four continuous PCET steps, CH_4 can be finally generated. By changing the pyrolysis temperature and coordination numbers of N, a series of Cu-based SACs with promising efficiency towards CH_4 have been prepared. Among them, isolated Cu–N_2 active sites have been shown to be favorable for CH_4 generation with the highest FE_{CH4} of 38.6% at −1.6 V *vs.* RHE.[129] Moreover, Han *et al.* designed ZnN_4 active sites anchored in microporous nitrogen-doped carbon, which reached a FE_{CH4} of 85%, inhibiting the reduction of CO_2 to CO.[130] Notice that on the ZnN_4 site, the rate-limiting step for the reduction of CO_2 to CH_4 was the transformation of *OCHOH to *CHO.

3. C1 products on MOF-derived SACs

SACs have been reported as effective catalysts due to their four-coordinated M-N_4 active sites with a symmetric coordination environment.[131–134] Due to their adjustable geometry and electronic properties, and the high exposure of active sites, M-N_4 moieties are considered one of the main active sites for eCO_2 RR catalytic performance. Therefore, it can be concluded that different activity and selectivity of the products are mainly influenced by the nature of the central metal atoms. Previous theoretical and experimental results proved that the metal-complex (M-N_4) site in SACs is the main active center of the catalytic reaction. Different central metals have different binding energies with intermediates such as *CO and *COOH, which may lead to different product selectivity. For example, Hu *et al.* supported that the selectivity and activity of M-N-C catalysts towards CO were generally ordered as Ni > Fe ≫ Co and Ni, Fe ≫ Co, respectively.[105] Different catalysts with M-N_4 active sites in a symmetric coordination environment have been reported for electrochemical CO_2-to-CO reaction, as shown in Table 2.

Table 2 eCO_2 RR performance of reported MOF-derived SACs with M-N_4 active sites

Configuration	Method	Main product	FE_{max}@potential (*vs.* RHE)	Ref.
Ni-N_4	MOF-derived	CO	71.9%@−0.89 V	68
Ni-N_4	MOF-derived	CO	98%@−1.0 V	138
Ni-N_4	MOF-derived	CO	97%@−0.9 V	139
Ni-N_4	MOF-derived	CO	96.2%@−1.0 V	140
Ni-N_4	MOF-derived	CO	96.8%@−0.8 V	141
Ni-N_4	MOF-derived	CO	97%@−0.79 V	142
Ni-N_4	MOF-derived	CO	92–98%@−1.03 V	143
Fe^{3+}-N_4	MOF-derived	CO	>80%@−0.47 V	42
Fe-N_4	MOF-derived	CO	94%@−0.46 V	144
Fe-N_4	MOF-derived	CO	>90%@−0.8 V	145
Co-N_4	MOF-derived	CO	82%@−1.0 V	146
Co-N_4	MOF-derived	CO	98.7%@−0.6 V	147
Cu-N_4	MOF-derived	CH_3OH	44%@−0.9 V	128
Cu-N_4/N_2	MOF-derived	C_2H_4	24%@−1.4 V	129
Cu-N_4	MOF-derived	C_2H_5OH	55%@−1.2 V	148
Cu-N_4	MOF-derived	CO	98%@−0.9 V	149
Co-N_4	MOF-derived	CO	82% @−0.8 V	146
Zn-N_3/N_4	MOF-derived	CO	100%@−0.57 V	49
In-N_4	MOF-derived	CO	97.2%@−0.7 V	150
In-N_4	MOF-derived	HCOOH	96%@−0.65 V	151
Bi-N_4	MOF-derived	CO	>97%	60
Ni-N_4/Cu-N_4	MOF-derived	CO	99%@−0.97 V	152

However, theoretical and experimental results revealed that the high structure/electron symmetry of the M-N_4 moiety, resulting from its symmetrical planar structure, makes it chemically inert to a certain extent, thus reducing the kinetics of the catalytic reaction and hindering it.[39,132,135,136] Therefore, in order to tune the performance of M-N_4 active sites for eCO_2 RR, breaking the symmetrical electronic structure of M-N_4 *via* a reasonable adjustment of the coordination structure to optimize the electronic structure of the M-N_4, and subsequently affecting the binding energies for eCO_2 RR intermediates have caught researchers' attention and have been developed in full swing. By tuning the coordination numbers and introducing second atoms (metal or non-metal), the d orbital of the metal site can be significantly tuned, affecting the catalytic activity for eCO_2 RR.[137] In the last few years, researchers have prepared a variety of novel SACs derived from MOFs, with most of them displaying more ideal eCO_2 RR performance. Therefore, in this section, we will discuss the influence of the alteration of coordination components, including M-N_x SACs, M-N_x-heteroatom SACs and M–M SACs, on the formation of different C1 products (Fig. 8).

3.1 M-$N_{x(x<4)}$

In most cases, SACs derived from MOFs form a stable M-N_4 coordination after pyrolysis at a high temperature due to their N-rich organic ligands. However, compared to traditional M-N_4 active sites, current works have revealed that the coordination number of the central metal atoms is also a key parameter, which affects the activation or intermediate dissociation of CO_2, thus giving us the possibility to tailor it in order to improve the catalytic activity and selectivity of SACs.[21,37,39,75,124] According to previous results, *via* adjusting the synthesis conditions, the number of nitrogen atoms coordinated with metal atoms could be regulated to realize M-$N_{x(1\le x\le 5)}$-C-like active sites, such as M-N_1/N_2/N_3/N_4/N_5-C.[153,154] Such regulated active sites can lead to a stronger or weaker interaction with the eCO_2 RR intermediate (*COOH or *CO), and thus exhibit higher or lower eCO_2 RR activity and selectivity. Especially, SACs with low coordination numbers exhibited higher catalytic performance towards CO generation. Generally, the pyrolysis temperature is one of the main conditions that we can modify in order to affect the coordination numbers of SACs (Fig. 9A). The nitrogen coordination number tends to gradually decrease with the increase of the pyrolysis temperature.[125] Furthermore, the formed M-N_x with defects can significantly improve the catalytic performance for eCO_2 RR. For example, Jiang *et al.* prepared MOF-74-derived Ni SA-N_2-C with lower N coordination numbers by controlling the pyrolysis temperature and achieved a high CO faradaic efficiency (98%) at −0.80 V *vs.* RHE and turnover frequency (1622 h^{-1}), which is better than the efficiency shown by similar metal catalysts with higher N coordination numbers (*e.g.* Ni SA-N_3-C and Ni SA-N_4-C) (Fig. 9B).[155] Theoretical calculations indicated that a lower

© 2023 The Author(s). Published by the Royal Society of Chemistry

Open Access Article. Published on 30 de novembre 2022. Downloaded on 27/1/2026 21:08:31.
This article is licensed under a Creative Commons Attribution 3.0 Unported Licence.

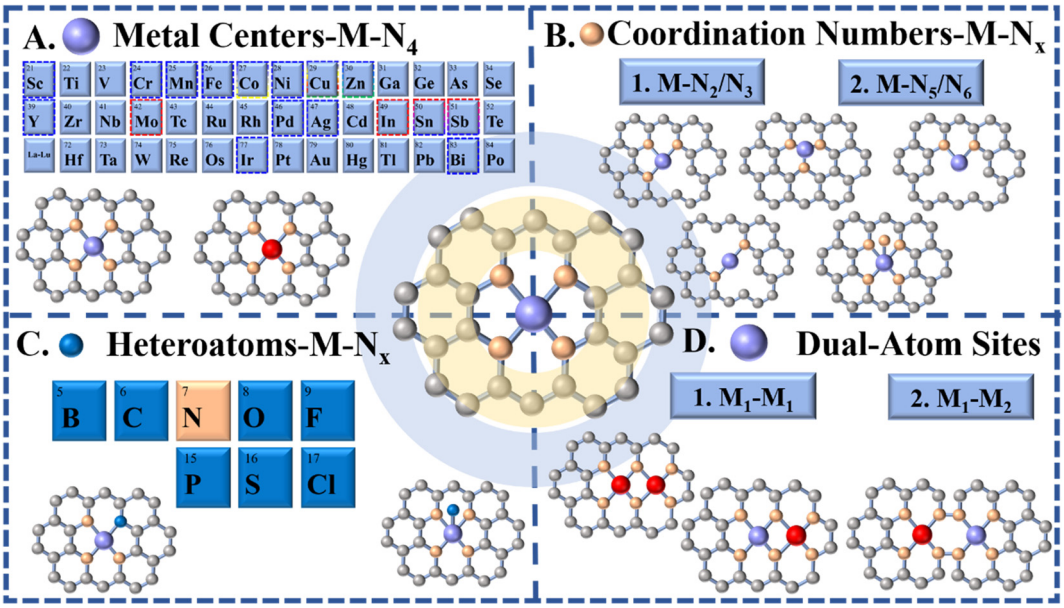

Fig. 8 Schematic illustration showing regulation of central metal atoms and the local atomic environment in M-N-C catalysts (C atoms: gray; N atoms: orange; metal atoms: purple/red; heteroatoms: blue).

coordination number could change the electronic structure of the active site, which is favorable to the formation of the COOH* intermediate, thereby enhancing the electroreduction activity of CO_2. Similarly, it has been shown that ZIF-8 derived FeN_3 active sites possess balanced adsorption energies for *COOH and *CO intermediates, facilitating CO formation, and thus, exhibiting superior eCO_2 RR performance with CO faradaic efficiency up to 96% at −0.5 V *vs.* RHE, a turnover frequency of 2225 h^{-1}, and an outstanding stability, which further support the superiority of M-N_x sites with low coordination numbers.[156] More importantly, the FeN_3 catalyst possessed excellent stability during the 48 h test. In addition, atomically dispersed Co active sites with two-coordinated nitrogen atoms, fabricated *via* pyrolysis of bimetallic Co/Zn ZIFs, showed high selectivity and superior activity with 94% FE(CO) at an overpotential of 520 mV as well as excellent stability (60 h). Such unsaturated Co-N_2 sites could promote the activation of CO_2 to the $CO_2^{\bullet-}$ intermediate and hence enhance the CO_2 electroreduction activity.[89] Effective conversion of CO_2 to CO on some Cu-N_4 active sites is more likely to occur.[149] Compared to Cu-N_4 active sites, the CO desorption on Cu-N_3 sites is difficult due to their high energy

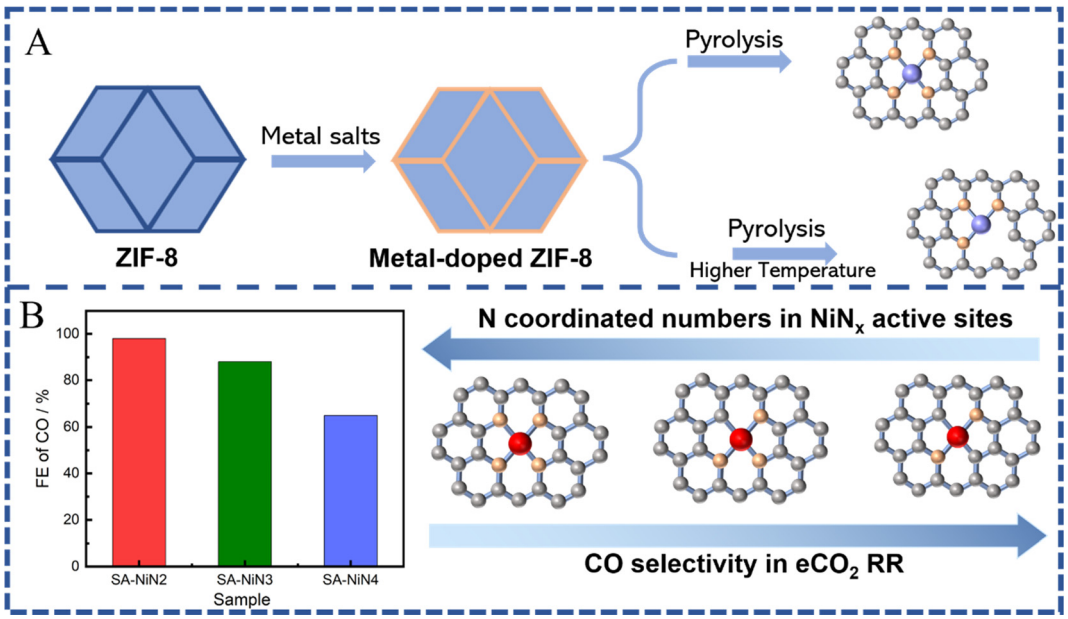

Fig. 9 (A) Schematic illustration of ZIF-8 derived SACs with different N coordination numbers (C atoms: gray; N atoms: orange; metal atoms: purple/red). (B) FE of CO (at −0.80 V *vs.* RHE) obtained on Ni-SACs with different N coordination numbers.

Open Access Article. Published on 30 de novembre 2022. Downloaded on 27/1/2026 21:08:31.
This article is licensed under a Creative Commons Attribution 3.0 Unported Licence.

barrier, leading to higher selectivity towards CH_4.[157,158] These results further confirm the promising use of MOFs for preparing low coordination number M-N_x sites, which facilitate the activation of CO_2-to-CO. For other C1 products, SACs with low coordination number M-N_x sites still show insufficient selectivity.

3.2 M-N_x-heteroatoms

Apart from the alteration of coordination numbers in SACs, the coordination environment of the metal centers is another important factor, which can also regulate the electronic and geometric structures of the SACs to influence the catalytic performance towards eCO_2 RR.[39,136,159,160] Due to the strong electronegative coordination of different heteroatoms, the strength of electronic metal–support interaction (EMSI) can be directly influenced, thus changing the valence electron distribution of SA sites, which can decrease the binding energy of the intermediates during the adsorption or desorption processes.[39,159] Based on this idea, in addition to the N atoms, the site modification by using some other hybrid coordinated atoms (O,[69,161,162] S,[163] or Cl,[164,165] among others) has also been investigated by researchers. The relative low electronegativity of the above mentioned hybrid coordinated atoms results in an electron transfer inside the active site of SACs with a heteroatom coordination, which consequently influences the binding energy for the different intermediates during their adsorption or desorption processes.[39] For example, Chen *et al.* introduced an axial Cl atom into the FeN_4 sites to modulate the electronic structure by following two steps: (1) pyrolyzing two-dimensional ZIF nanosheets with loaded Fe and (2) performing a low-temperature incubation in hydrochloric acid solution. The obtained FeN_4Cl active sites facilitated the desorption of CO* and inhibited the adsorption of H*, resulting in an improved FE(CO) of 90.5% and a low overpotential of 490 mV in eCO_2 RR.[164] Sn-based SACs consisting of atomically dispersed SnN_3O_1 active sites supported on a N-rich carbon matrix (Sn-NOC) were also prepared for efficient eCO_2 RR. Compared to the classic Sn-N_4 configuration, which produced HCOOH and H_2 as predominant products, SnN_3O_1 generated CO as the main product with a FE_{CO} of 94% at −0.7 V *vs.* RHE. DFT calculations showed that the atomic arrangement of SnN_3O_1 reduces the activation energy for *COO and *COOH formation, while increasing the energy barrier for HCOO* formation significantly, thereby facilitating CO_2-to-CO conversion and suppressing HCOOH production.[59] The axial halogen atoms with distinct electronegativity can break the symmetric charge distribution of MN_4 active sites and facilitate the *COOH formation, leading to high selectivity towards CO.[165] Therefore, a series of Ni-SACs with different halogen doping atoms were prepared by the pyrolysis of ZIF-8, in which due to the most electronegative Cl atoms, NiNC-Cl exhibited the highest FE of CO (94.7%), outperforming NiNC-Br and NiNC-I samples. DFT calculations revealed that the axial coordinated halogen atoms could facilitate *COOH formation, thereby boosting the CO_2 reduction reaction (Fig. 10). In addition to the two-step introduction, the coordination of heteroatoms can be easily achieved after pyrolysis *via* the rational design of organic linkers with functional groups, providing a feasible strategy to dope the hybrid atoms into the SACs. Following the above idea, we have recently reported a facile route *via* using oxygen- and nitrogen-rich MOFs (IRMOF-3) as precursors to obtain the Fe–O and Fe–N chelation simultaneously, resulting in atomically dispersed axial O-coordinated FeN_4 active sites.[69] Compared to the FeN_4 active sites without O coordination, the formed FeN_4-O sites exhibit much better catalytic performance toward CO, reaching a maximum FE_{CO} of 95% at −0.50 V *versus* RHE and 30 h stability. Density functional theory calculations indicated

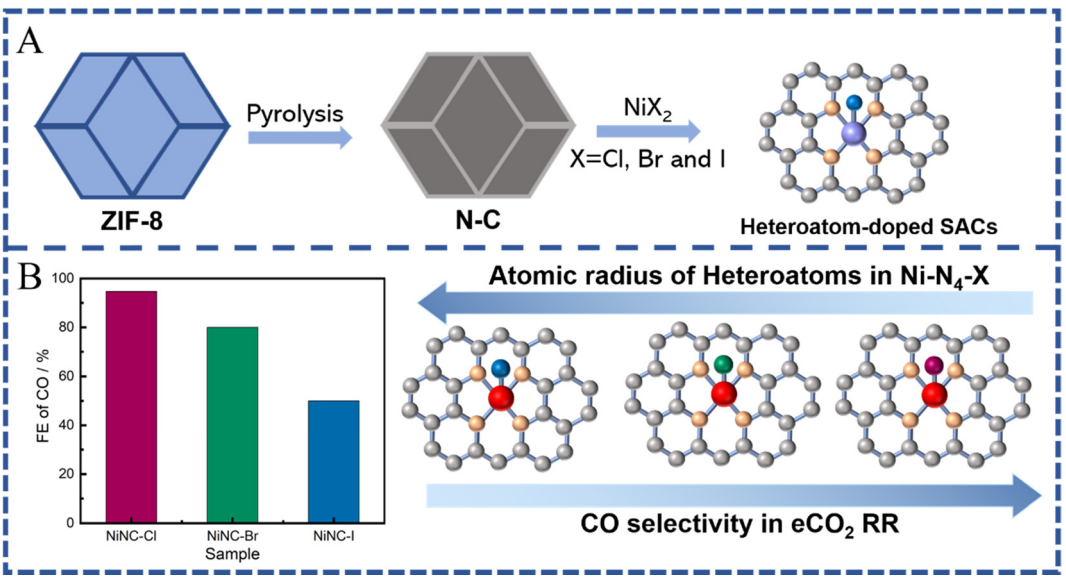

Fig. 10 (A) Schematic illustration of ZIF-8 derived SACs with different heteroatom dopants (C atoms: gray; N atoms: orange; metal atoms: purple/red; heteroatoms: blue). (B) FE of CO (at −0.7 V *vs.* RHE) obtained on Ni-SACs with different heteroatom dopants (C atoms: gray; N atoms: orange; Ni atoms: red; Cl atom: dark red; Br atom: green; I atom: dark blue).

© 2023 The Author(s). Published by the Royal Society of Chemistry

Open Access Article. Published on 30 de novembre 2022. Downloaded on 27/1/2026 21:08:31. This article is licensed under a Creative Commons Attribution 3.0 Unported Licence.

that the axial O-coordination regulates the binding energy of intermediates in the reaction pathways, resulting in a smoother desorption of CO and increased energy for the competitive hydrogen production.[69] Similarly, the introduction of oxygen ligands also brought remarkably high FE (78%) for the electrochemical conversion of CO_2 to CH_4 on Cu-SACs, surpassing most of the reported SACs, which stop at two-electron transfer related reduction processes. Theoretical calculations revealed that the high selectivity on formed CuN_2O_2 active sites with an oxygen ligand is due to the properly elevated CH_4 and H_2 energy barriers and the fine-tuned electronic structure of the Cu active sites.[47] In summary, precisely controlling the coordination environment of SACs by heteroatom dopants has a significant effect on the catalytic performance towards eCO_2 RR.

3.3 M-M SACs

Although several reported monometallic active sites have already exhibited high selectivity for CO, they still suffer from sluggish kinetics for different steps of the eCO_2 RR. For instance, Fe-N_4 and Co-N_4 sites have shown low onset potential for CO_2 RR because of favorable kinetics for *COOH formation, but a relatively low FE for CO due to the strong binding energy of CO to the single Fe- or Co-atom sites.[70,166–169] In addition, traditional SACs are sporadically dispersed on substrates without interaction between each other, leading to problems for C–C coupling reactions during eCO_2 RR. To address the above issues, the design and synthesis of a multi-metal active center, possessing flexible active centers and synergy between adjacent metal sites, can bring unexpected catalytic performance to SACs.[170–172] With potential abundant metal sites and nanopores, MOFs are certified as ideal templates for stabilizing and preparing dual-atom metal sites. In this section, MOF-derived dual-active sites will be divided into two types including binuclear homologous dual active sites (M1–M1) and binuclear heterologous dual active sites (M1–M2).

3.3.1 M1–M1 SACs. M1–M1 binuclear homologous SACs are composed of two identical active sites anchored on the substrate with or without metal–metal bonds. These M1–M1 SACs can play a role in modifying the properties of metal atoms by using the same metal atom species in a homonuclear bimetallic site. In this way, they are emerging as promising candidates to effectively influence the electrochemical reactions by adjusting the geometric and electronic structures of the catalytic sites, changing the energy barrier in the reaction process.[173] Zhao *et al.* investigated Cu dimers embedded in C_2N layers, showing a superior performance for converting CO_2 to CH_4 ($CO_2 \rightarrow HCOO^* \rightarrow HCOOH^* \rightarrow H_2COOH^* \rightarrow H_2CO^* \rightarrow H_2COH^* \rightarrow CH_2^* \rightarrow CH_3^* \rightarrow CH_4$).[174] In addition, Guan *et al.* reported Cu-based SACs with C_2H_4 selectivity. In the latter case, when the Cu concentration was low ($2.4\%_{mol}$), highly dispersed Cu active sites resulted in the formation of CH_4, while when increasing the Cu concentration to $4.9\%_{mol}$, abundant Cu active sites were close enough to result in the dimerization of the *CO intermediates, achieving C_2H_4 selectivity.[129] A diatomic electrocatalyst with homonuclear Fe_2N_6 sites was successfully prepared through pyrolysis of the $Fe_2(CO)_9$ containing ZIF-8 precursor for efficiently reducing CO_2 to CO. Such diatomic catalyst achieved CO FE up to 96.0% at −0.60 V *vs.* RHE, much superior to the single-atom Fe catalyst counterpart.[175] DFT calculations revealed that neighboring Fe–Fe centers facilitate the CO_2 activation process *via* concurrently bonding the C and O atoms of the CO_2 molecule. Furthermore, the reaction barrier of CO desorption on the bimetallic sites was decreased by the synergy of the dual Fe center.

3.3.2 M1–M2 SACs. Adjacent M_1–N_4 and M_2–N_4 active sites anchored on carbon substrates with or without M1–M2 metal bonds form the binuclear heterologous site catalysts.[37,168,176] The incorporation of the second metal induces a synergetic catalytic effect on M1–M2 active sites. By the pyrolysis of ZIF-8 assembled with Fe and Ni-doped ZnO nanoparticles, a Ni/Fe-N-C catalyst composed of neighboring Fe and Ni was precisely constructed by Jiao *et al.*[93] Owing to the synergism of neighboring Fe and Ni active sites, Ni/Fe-N-C presented a boosted performance for eCO_2 RR, which far surpassed the performance of the single Fe-N-C and Ni-N-C SAC counterparts. DFT calculations revealed that the presence of Fe adjacent to the Ni active sites can facilitate the formation of the COOH* intermediate and thereby accelerate the CO_2 reduction (Fig. 11). In addition, with the aid of a MOF template, a Ni/Cu dual-site catalyst with well-defined coordination was successfully synthesized.[177] The synergistic effect of adjacent Ni-N_4 and Cu-N_4 active sites could adjust the distribution of electrons and reduce the band gap and the overall potential barrier of the CO_2 RR, resulting in a remarkable catalytic performance. Combining Co single-atom sites with Fe single-atom sites derived from MOFs, the bimetallic CoPc@Fe-NC SAC showed significantly broad potential windows for CO generation in comparison to the two single metal site counterparts. What is more, the maximum CO current density was increased ten times with significantly enhanced stability (20 h). Density functional theory calculations suggested that the anchored cobalt phthalocyanine promotes the CO desorption and suppresses the competitive hydrogen evolution reaction over Fe-N sites, while the *COOH formation remains almost unchanged, thus demonstrating unprecedented synergistic effect toward eCO_2 RR.[178] With the help of a Zn-based MOF assisted method, we prepared a quasi-double star catalyst composed of nearby Ni and Fe single-atom active sites acting as a combined nanoreactor.[70] Specifically, the optimized Ni/Fe-N-C catalyst showed exclusive selectivity (with a maximum FE(CO) of 98%) at a low overpotential of 390 mV *vs.* RHE, which was superior to both the single metal counterparts (Ni-N-C and Fe-N-C catalysts). In addition, such dual-metal sites composed of Ni and Fe showed good stability up to 30 h. The DFT results further revealed that regulating the catalytic CO_2 RR performance *via* nearby Ni and Fe active sites can potentially break the activity benchmark of the single metal counterparts because the neighboring Ni and Fe active sites not only function in synergy to decrease the reaction barrier for the formation of COOH* and desorption of CO* in comparison to their single metal counterparts, but also prevent the undesired hydrogen evolution reaction (HER). In addition, Xie *et al.* prepared a ZIF-8 nanoarray as a precursor to construct a Ni-Sn atom pair electrocatalyst after pyrolysis. This N_4-Ni-Sn-N_4 coordination

Open Access Article. Published on 30 de novembre 2022. Downloaded on 27/1/2026 21:08:31.
This article is licensed under a Creative Commons Attribution 3.0 Unported Licence.

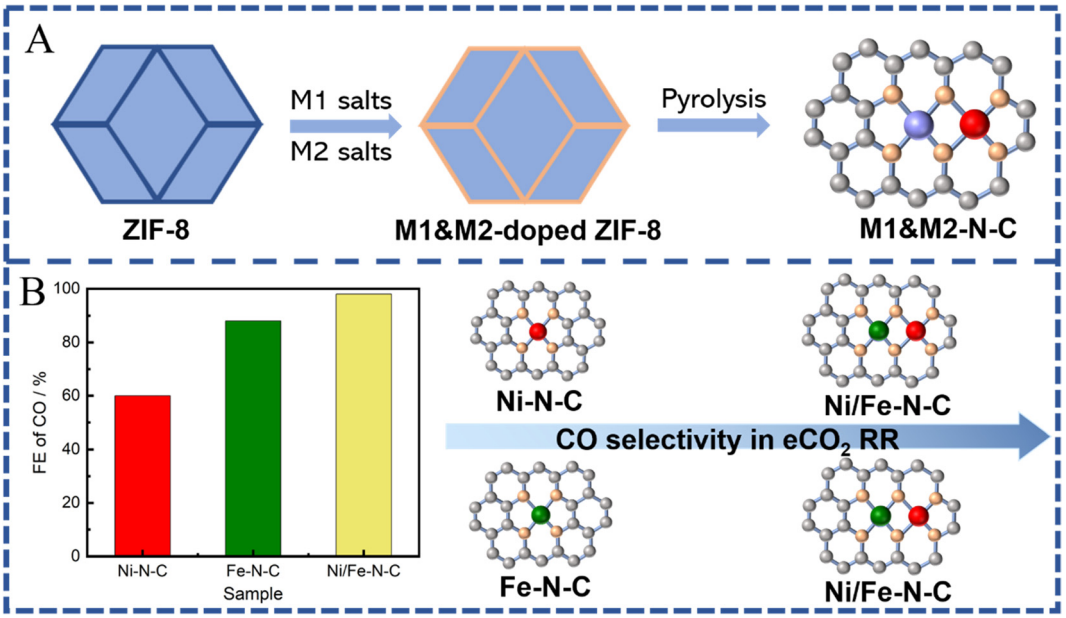

Fig. 11 (A) Schematic illustration of ZIF-8 derived SACs with two metal sites (C atoms: gray; N atoms: orange; metal atoms: purple/red; heteroatoms: blue). (B) FE of CO (at −0.50 V *vs.* RHE) obtained on Ni-N-C, Fe-N-C and Ni/Fe-N-C samples (C atoms: gray; N atoms: orange; Ni atoms: red; Fe atom: green).

configuration promoted the selectivity toward HCOOH (86.1%) at −0.82 V *vs.* RHE with 23 h stability in comparison to the two single atom counterparts.[179] Experiments and theoretical calculations further confirmed that the existence of bimetallic N_4-Ni-Sn-N_4 sites can influence the electron redistribution, thereby lowering the generation energy barrier of the *OCHO intermediate in eCO_2 RR, and making this potential-determining step thermodynamically spontaneous. Combining a Co-based molecular catalyst with Zn-based SACs derived from ZIF-8, a tandem catalyst was constructed by Lin *et al.* for eCO_2 RR to CH_4.[180] The selectivity of CH_4 was much higher than that found on single component catalysts, because CO_2 was first reduced to CO on CoPc, and the formed CO subsequently diffused to the Zn-N_4 site for further being reduced to CH_4. By DFT calculations, CoPc played a key role, which not only generated CO, but also improved the utilization of *H in this tandem catalyst, thereby leading to the selectivity of CH_4. These works demonstrated that due to the unique orbital and geometric configuration of bimetallic active sites, the energy barrier of different intermediates in catalytic eCO_2 RR can be lowered and thus the final reactions improved.

4. Summary and outlook

Benefiting from their high-efficiency catalytic ability, SACs derived from MOFs are one of the most promising electrocatalyst types. In fact, they are expected to replace traditional metal catalysts for eCO_2 RR. By using strategies that can regulate the electronic structure, the binding energy of adsorption/desorption for intermediates can be effectively adjusted and the energy barrier can be lowered, thus tuning the selectivity to achieve the targeted product. Although much progress has been made in the field of SAC preparation, many challenges remain. Firstly, from the practical application, the scaling up of synthesis strategies with commercial reactants and under lower temperature conditions needs to be further developed. The inferior accessibility due to the low density of single-atom active sites significantly hampers the catalytic performance in SACs. Increasing the metal load while avoiding agglomeration will be a bottleneck that needs to be surpassed in the development of new synthesis methods. In this exploration, we believe that the utilization of MOFs is, in this way, an attractive strategy. In addition, the enhancement of the intrinsic activity of the single-atom sites could also promote a better catalytic performance. The choice of the metal center and the regulation of its geometric and electronic environment will still be a key point to optimize the adsorption/desorption energy of the intermediates during eCO_2 RR. In this way, the varied porous architectures and environment of MOFs provide more possibilities for enhancing the intrinsic nature of the single-atom sites.

For the SACs derived from MOFs, some points still need to be given more attention during the design: (1) more suitable MOFs with a precise structure and a variety of functional groups are highly needed for creating SACs. (2) Heteroatom coordinated SACs should also be developed through heteroatom-rich MOF precursors to overcome the limitation from N-coordinated SAC materials. (3) Due to their complicated synthesis, the high price of ligands, and the limited stability of MOFs, we should also focus on the improved development of MOF precursors.

In addition, developing accurate characterization methodologies is urgently needed in order to better understand the local structure of SACs. In this way, for most of the available characterization methods, precise characterization down to the atomic scale still remains a challenge. The average structure rather than the local structure brings more uncertainties in the

© 2023 The Author(s). Published by the Royal Society of Chemistry

Open Access Article. Published on 30 de novembre 2022. Downloaded on 27/1/2026 21:08:31.
This article is licensed under a Creative Commons Attribution 3.0 Unported Licence.

optimization of the preparation process. Moreover, without a clear knowledge of the nature of the active sites, research about catalytic mechanisms and theoretical computation is in a quandary. To understand the nature of single-atom sites and explore their reaction mechanisms, we will need to combine different advanced characterization methodologies, such as electron related microscopy and spectroscopy at the nano- and atomic scale with synchrotron X-ray experiments, and even take advantage of theoretical simulations (*e.g.* DFT) and artificial intelligence (AI) automated data analysis.[181–183]

Furthermore, we should take into account that during reaction processes, the environment around the active sites has dynamic variations, which have impacts on the properties of these active sites. *In situ* and operando techniques, such as *in situ* electron microscopy, *in situ* X-ray absorption spectroscopy and *in situ* X-ray photoelectron spectroscopy, may help to unearth SACs' properties, which change during the catalytic reactions, to gain a comprehensive understanding of the catalysts and reaction mechanisms.

Likewise, as most of the current research on SACs has been limited to C1 products, more complex and higher value products should be explored. For more complex C2 products, which include more intermediates, protonation and electron transfers, the separated SACs serving as an optimized active site for a single process could not implement the multiple-intermediate conversion processes. We have shown that dual- and multiple-atom sites can show catalytic synergistic effects. Therefore, these synergistic properties should be used to achieve the more complex C2 product transformation. Additionally, the substrates interacting with SACs could regulate their geometric and electronic structure *via* the functionalization of the substrate precursor.

Finally, most of the SACs have shown their eCO_2 RR performance in H-cells. The low solubility of CO_2 in aqueous-fed systems limits the current density of CO_2 conversion to less than 35 mA cm^{-2} which could not satisfy the requirements for industrial application. Additionally, the optimization of the catalysts only at low current density may improve the catalyst only for the wrong environment. Using flow cells with a gas-diffusion layer could increase the current densities under a more realistic operating condition.

From our point of view, all the above progress will contribute in the future to the final optimization of the eCO_2 RR to meet large-scale industrial production.

Conflicts of interest

There are no conflicts to declare.

Acknowledgements

ICN2 acknowledges funding from Generalitat de Catalunya 2017 SGR 327. This study was supported by MCIN with funding from European Union NextGenerationEU (PRTR-C17.I1) and Generalitat de Catalunya. The authors acknowledge support from the project NANOGEN (PID2020-116093RB-C43), funded by MCIN/AEI/10.13039/501100011033/and by ''ERDF A way of making Europe'', by the ''European Union''. ICN2 is supported by the Severo Ochoa program from Spanish MCIN/AEI (Grant No. CEX2021-001214-S) and is funded by the CERCA Programme/Generalitat de Catalunya.

References

1 D. Voiry, H. S. Shin, K. P. Loh and M. Chhowalla, *Nat. Rev. Chem.*, 2018, **2**, 0105.
2 G. Wang, J. Chen, Y. Ding, P. Cai, L. Yi, Y. Li, C. Tu, Y. Hou, Z. Wen and L. Dai, *Chem. Soc. Rev.*, 2021, **50**, 4993–5061.
3 S. Navarro-Jaén, M. Virginie, J. Bonin, M. Robert, R. Wojcieszak and A. Y. Khodakov, *Nat. Rev. Chem.*, 2021, **5**, 564–579.
4 M. Ding, R. W. Flaig, H.-L. Jiang and O. M. Yaghi, *Chem. Soc. Rev.*, 2019, **48**, 2783–2828.
5 J. Qiao, Y. Liu, F. Hong and J. Zhang, *Chem. Soc. Rev.*, 2014, **43**, 631–675.
6 P. Zhang, J. Tong and K. Huang, *Materials and Processes for CO_2* Capture, Conversion, and Sequestration, 2018, pp. 213–266, DOI: 10.1002/9781119231059.ch5.
7 R. Snoeckx and A. Bogaerts, *Chem. Soc. Rev.*, 2017, **46**, 5805–5863.
8 S. C. Shit, I. Shown, R. Paul, K.-H. Chen, J. Mondal and L.-C. Chen, *Nanoscale*, 2020, **12**, 23301–23332.
9 J.-P. Jones, G. K. S. Prakash and G. A. Olah, *Isr. J. Chem.*, 2014, **54**, 1451–1466.
10 Z. Yuan, M. R. Eden and R. Gani, *Ind. Eng. Chem. Res.*, 2016, **55**, 3383–3419.
11 J. Liu, C. Guo, A. Vasileff and S. Qiao, *Small Methods*, 2017, **1**, 1600006.
12 Y. Wu, S. Cao, J. Hou, Z. Li, B. Zhang, P. Zhai, Y. Zhang and L. Sun, *Adv. Energy Mater.*, 2020, **10**, 2000588.
13 Y. Wang, P. Han, X. Lv, L. Zhang and G. Zheng, *Joule*, 2018, **2**, 2551–2582.
14 D. D. Zhu, J. L. Liu and S. Z. Qiao, *Adv. Mater.*, 2016, **28**, 3423–3452.
15 L. Zhang, Z.-J. Zhao and J. Gong, *Angew. Chem., Int. Ed.*, 2017, **56**, 11326–11353.
16 A. D. Handoko, F. Wei, Jenndy, B. S. Yeo and Z. W. Seh, *Nat. Catal.*, 2018, **1**, 922–934.
17 Y. Zheng, A. Vasileff, X. Zhou, Y. Jiao, M. Jaroniec and S.-Z. Qiao, *J. Am. Chem. Soc.*, 2019, **141**, 7646–7659.
18 X. Han, T. Zhang, M. Biset-Peiró, X. Zhang, J. Li, W. Tang, P. Tang, J. R. Morante and J. Arbiol, *ACS Appl. Mater. Interfaces*, 2022, **14**, 32157–32165.
19 S. Jin, Z. Hao, K. Zhang, Z. Yan and J. Chen, *Angew. Chem., Int. Ed.*, 2021, **60**, 20627–20648.
20 E. E. Benson, C. P. Kubiak, A. J. Sathrum and J. M. Smieja, *Chem. Soc. Rev.*, 2009, **38**, 89–99.
21 Q. Sun, C. Jia, Y. Zhao and C. Zhao, *Chin. J. Catal.*, 2022, **43**, 1547–1597.
22 C. S. Diercks, Y. Liu, K. E. Cordova and O. M. Yaghi, *Nat. Mater.*, 2018, **17**, 301–307.

© 2023 The Author(s). Published by the Royal Society of Chemistry

Open Access Article. Published on 30 de novembre 2022. Downloaded on 27/1/2026 21:08:31.
This article is licensed under a Creative Commons Attribution 3.0 Unported Licence.

23 Y.-J. Zhang, V. Sethuraman, R. Michalsky and A. A. Peterson, *ACS Catal.*, 2014, **4**, 3742–3748.
24 B. Qiao, A. Wang, X. Yang, L. F. Allard, Z. Jiang, Y. Cui, J. Liu, J. Li and T. Zhang, *Nat. Chem.*, 2011, **3**, 634–641.
25 X.-F. Yang, A. Wang, B. Qiao, J. Li, J. Liu and T. Zhang, *Acc. Chem. Res.*, 2013, **46**, 1740–1748.
26 L. Liu and A. Corma, *Chem. Rev.*, 2018, **118**, 4981–5079.
27 X. Wang, Y. Zhang, J. Wu, Z. Zhang, Q. Liao, Z. Kang and Y. Zhang, *Chem. Rev.*, 2022, **122**, 1273–1348.
28 M. B. Gawande, P. Fornasiero and R. Zbořil, *ACS Catal.*, 2020, **10**, 2231–2259.
29 D. Zhao, Z. Zhuang, X. Cao, C. Zhang, Q. Peng, C. Chen and Y. Li, *Chem. Soc. Rev.*, 2020, **49**, 2215–2264.
30 B. Chang, L. Zhang, S. Wu, Z. Sun and Z. Cheng, *Chem. Soc. Rev.*, 2022, **51**, 3688–3734.
31 J. Xia, B. Wang, J. Di, Y. Li, S.-Z. Yang, H. Li and S. Guo, *Mater. Today*, 2022, **53**, 217–237.
32 Y. Yang, Y. Yang, Z. Pei, K.-H. Wu, C. Tan, H. Wang, L. Wei, A. Mahmood, C. Yan, J. Dong, S. Zhao and Y. Chen, *Matter*, 2020, **3**, 1442–1476.
33 Y. Wang, H. Su, Y. He, L. Li, S. Zhu, H. Shen, P. Xie, X. Fu, G. Zhou, C. Feng, D. Zhao, F. Xiao, X. Zhu, Y. Zeng, M. Shao, S. Chen, G. Wu, J. Zeng and C. Wang, *Chem. Rev.*, 2020, **120**, 12217–12314.
34 X. Li, L. Liu, X. Ren, J. Gao, Y. Huang and B. Liu, *Sci. Adv.*, 2020, **6**, eabb6833.
35 T. N. Nguyen, M. Salehi, Q. V. Le, A. Seifitokaldani and C. T. Dinh, *ACS Catal.*, 2020, **10**, 10068–10095.
36 L. Wang, W. Chen, D. Zhang, Y. Du, R. Amal, S. Qiao, J. Wu and Z. Yin, *Chem. Soc. Rev.*, 2019, **48**, 5310–5349.
37 D. Zhou, X. Li, H. Shang, F. Qin and W. Chen, *J. Mater. Chem. A*, 2021, **9**, 23382–23418.
38 F. Doherty, H. Wang, M. Yang and B. R. Goldsmith, *Catal. Sci. Technol.*, 2020, **10**, 5772–5791.
39 Q. Qu, S. Ji, Y. Chen, D. Wang and Y. Li, *Chem. Sci.*, 2021, **12**, 4201–4215.
40 Y. Pan, R. Lin, Y. Chen, S. Liu, W. Zhu, X. Cao, W. Chen, K. Wu, W.-C. Cheong, Y. Wang, L. Zheng, J. Luo, Y. Lin, Y. Liu, C. Liu, J. Li, Q. Lu, X. Chen, D. Wang, Q. Peng, C. Chen and Y. Li, *J. Am. Chem. Soc.*, 2018, **140**, 4218–4221.
41 H.-n Zhang, H.-q Wang, S.-p Jia, Q. Chang, N. Li, Y. Li, X.-l Shi, Z.-y Li and S.-l Hu, *New Carbon Mater.*, 2022, **37**, 734–742.
42 J. Gu, C.-S. Hsu, L. Bai, H. M. Chen and X. Hu, *Science*, 2019, **364**, 1091–1094.
43 X. Qin, S. Zhu, F. Xiao, L. Zhang and M. Shao, *ACS Energy Lett.*, 2019, **4**, 1778–1783.
44 H. B. Yang, S.-F. Hung, S. Liu, K. Yuan, S. Miao, L. Zhang, X. Huang, H.-Y. Wang, W. Cai, R. Chen, J. Gao, X. Yang, W. Chen, Y. Huang, H. M. Chen, C. M. Li, T. Zhang and B. Liu, *Nat. Energy*, 2018, **3**, 140–147.
45 X. Rong, H.-J. Wang, X.-L. Lu, R. Si and T.-B. Lu, *Angew. Chem., Int. Ed.*, 2020, **59**, 1961–1965.
46 J. Jiao, R. Lin, S. Liu, W.-C. Cheong, C. Zhang, Z. Chen, Y. Pan, J. Tang, K. Wu, S.-F. Hung, H. M. Chen, L. Zheng, Q. Lu, X. Yang, B. Xu, H. Xiao, J. Li, D. Wang, Q. Peng, C. Chen and Y. Li, *Nat. Chem.*, 2019, **11**, 222–228.
47 Y. Cai, J. Fu, Y. Zhou, Y.-C. Chang, Q. Min, J.-J. Zhu, Y. Lin and W. Zhu, *Nat. Commun.*, 2021, **12**, 586.
48 F. Yang, P. Song, X. Liu, B. Mei, W. Xing, Z. Jiang, L. Gu and W. Xu, *Angew. Chem., Int. Ed.*, 2018, **57**, 12303–12307.
49 S. Li, S. Zhao, X. Lu, M. Ceccato, X.-M. Hu, A. Roldan, J. Catalano, M. Liu, T. Skrydstrup and K. Daasbjerg, *Angew. Chem., Int. Ed.*, 2021, **60**, 22826–22832.
50 S. Baskaran and J. Jung, *Appl. Surf. Sci.*, 2022, **592**, 153339.
51 P. Huang, M. Cheng, H. Zhang, M. Zuo, C. Xiao and Y. Xie, *Nano Energy*, 2019, **61**, 428–434.
52 Q. He, J. H. Lee, D. Liu, Y. Liu, Z. Lin, Z. Xie, S. Hwang, S. Kattel, L. Song and J. G. Chen, *Adv. Funct. Mater.*, 2020, **30**, 2000407.
53 N. Zhang, X. Zhang, Y. Kang, C. Ye, R. Jin, H. Yan, R. Lin, J. Yang, Q. Xu, Y. Wang, Q. Zhang, L. Gu, L. Liu, W. Song, J. Liu, D. Wang and Y. Li, *Angew. Chem., Int. Ed.*, 2021, **60**, 13388–13393.
54 J. Bok, S. Y. Lee, B.-H. Lee, C. Kim, D. L. T. Nguyen, J. W. Kim, E. Jung, C. W. Lee, Y. Jung, H. S. Lee, J. Kim, K. Lee, W. Ko, Y. S. Kim, S.-P. Cho, J. S. Yoo, T. Hyeon and Y. J. Hwang, *J. Am. Chem. Soc.*, 2021, **143**, 5386–5395.
55 N. Zhang, X. Zhang, L. Tao, P. Jiang, C. Ye, R. Lin, Z. Huang, A. Li, D. Pang, H. Yan, Y. Wang, P. Xu, S. An, Q. Zhang, L. Liu, S. Du, X. Han, D. Wang and Y. Li, *Angew. Chem., Int. Ed.*, 2021, **60**, 6170–6176.
56 Y. Li, C. Chen, R. Cao, Z. Pan, H. He and K. Zhou, *Appl. Catal. B: Environ.*, 2020, **268**, 118747.
57 W. Ni, Y. Gao, Y. Lin, C. Ma, X. Guo, S. Wang and S. Zhang, *ACS Catal.*, 2021, **11**, 5212–5221.
58 X. Zu, X. Li, W. Liu, Y. Sun, J. Xu, T. Yao, W. Yan, S. Gao, C. Wang, S. Wei and Y. Xie, *Adv. Mater.*, 2019, **31**, 1808135.
59 J. Guo, W. Zhang, L.-H. Zhang, D. Chen, J. Zhan, X. Wang, N. R. Shiju and F. Yu, *Adv. Sci.*, 2021, **8**, 2102884.
60 E. Zhang, T. Wang, K. Yu, J. Liu, W. Chen, A. Li, H. Rong, R. Lin, S. Ji, X. Zheng, Y. Wang, L. Zheng, C. Chen, D. Wang, J. Zhang and Y. Li, *J. Am. Chem. Soc.*, 2019, **141**, 16569–16573.
61 C.-C. Hou, H.-F. Wang, C. Li and Q. Xu, *Energy Environ. Sci.*, 2020, **13**, 1658–1693.
62 Y. Chen, S. Ji, C. Chen, Q. Peng, D. Wang and Y. Li, *Joule*, 2018, **2**, 1242–1264.
63 L. Jiao and H.-L. Jiang, *Chem*, 2019, **5**, 786–804.
64 X. Liang, S. Ji, Y. Chen and D. Wang, *iScience*, 2022, **25**, 104177.
65 Q. Fu, H. Saltsburg and M. Flytzani-Stephanopoulos, *Science*, 2003, **301**, 935–938.
66 S. F. J. Hackett, R. M. Brydson, M. H. Gass, I. Harvey, A. D. Newman, K. Wilson and A. F. Lee, *Angew. Chem., Int. Ed.*, 2007, **46**, 8593–8596.
67 S. Sun, G. Zhang, N. Gauquelin, N. Chen, J. Zhou, S. Yang, W. Chen, X. Meng, D. Geng, M. N. Banis, R. Li, S. Ye, S. Knights, G. A. Botton, T.-K. Sham and X. Sun, *Sci. Rep.*, 2013, **3**, 1775.
68 C. Zhao, X. Dai, T. Yao, W. Chen, X. Wang, J. Wang, J. Yang, S. Wei, Y. Wu and Y. Li, *J. Am. Chem. Soc.*, 2017, **139**, 8078–8081.

© 2023 The Author(s). Published by the Royal Society of Chemistry

Open Access Article. Published on 30 de novembre 2022. Downloaded on 27/1/2026 21:08:31.
This article is licensed under a Creative Commons Attribution 3.0 Unported Licence.

69 T. Zhang, X. Han, H. Liu, M. Biset-Peiró, J. Li, X. Zhang, P. Tang, B. Yang, L. Zheng, J. R. Morante and J. Arbiol, *Adv. Funct. Mater.*, 2022, **32**, 2111446.
70 T. Zhang, X. Han, H. Liu, M. Biset-Peiró, X. Zhang, P. Tan, P. Tang, B. Yang, L. Zheng, J. R. Morante and J. Arbiol, *Energy Environ. Sci.*, 2021, **14**, 4847–4857.
71 J. Gao, Y. Hu, Y. Wang, X. Lin, K. Hu, X. Lin, G. Xie, X. Liu, K. M. Reddy, Q. Yuan and H.-J. Qiu, *Small*, 2021, **17**, 2104684.
72 J. Ye, J. Yan, Y. Peng, F. Li and J. Sun, *Catal. Today*, 2023, **410**, 68–84.
73 S. S. A. Shah, T. Najam, M. Wen, S.-Q. Zang, A. Waseem and H.-L. Jiang, *Small Struct.*, 2022, **3**, 2100090.
74 Y.-Z. Chen, R. Zhang, L. Jiao and H.-L. Jiang, *Coord. Chem. Rev.*, 2018, **362**, 1–23.
75 Z. Song, L. Zhang, K. Doyle-Davis, X. Fu, J.-L. Luo and X. Sun, *Adv. Energy Mater.*, 2020, **10**, 2001561.
76 H. Huang, K. Shen, F. Chen and Y. Li, *ACS Catal.*, 2020, **10**, 6579–6586.
77 H.-L. Jiang, B. Liu, Y.-Q. Lan, K. Kuratani, T. Akita, H. Shioyama, F. Zong and Q. Xu, *J. Am. Chem. Soc.*, 2011, **133**, 11854–11857.
78 L. Jiao, G. Wan, R. Zhang, H. Zhou, S.-H. Yu and H.-L. Jiang, *Angew. Chem., Int. Ed.*, 2018, **57**, 8525–8529.
79 L. Jiao, R. Zhang, G. Wan, W. Yang, X. Wan, H. Zhou, J. Shui, S.-H. Yu and H.-L. Jiang, *Nat. Commun.*, 2020, **11**, 2831.
80 W. Chen, J. Pei, C.-T. He, J. Wan, H. Ren, Y. Wang, J. Dong, K. Wu, W.-C. Cheong, J. Mao, X. Zheng, W. Yan, Z. Zhuang, C. Chen, Q. Peng, D. Wang and Y. Li, *Adv. Mater.*, 2018, **30**, 1800396.
81 A. Han, B. Wang, A. Kumar, Y. Qin, J. Jin, X. Wang, C. Yang, B. Dong, Y. Jia, J. Liu and X. Sun, *Small Methods*, 2019, **3**, 1800471.
82 J. Hwang, *Korean J. Chem. Eng.*, 2021, **38**, 1104–1116.
83 Q. Yang, C.-C. Yang, C.-H. Lin and H.-L. Jiang, *Angew. Chem., Int. Ed.*, 2019, **58**, 3511–3515.
84 A. Zitolo, V. Goellner, V. Armel, M.-T. Sougrati, T. Mineva, L. Stievano, E. Fonda and F. Jaouen, *Nat. Mater.*, 2015, **14**, 937–942.
85 Y. Yang, K. Mao, S. Gao, H. Huang, G. Xia, Z. Lin, P. Jiang, C. Wang, H. Wang and Q. Chen, *Adv. Mater.*, 2018, **30**, 1801732.
86 L. Fan, P. F. Liu, X. Yan, L. Gu, Z. Z. Yang, H. G. Yang, S. Qiu and X. Yao, *Nat. Commun.*, 2016, **7**, 10667.
87 Y.-Z. Chen, C. Wang, Z.-Y. Wu, Y. Xiong, Q. Xu, S.-H. Yu and H.-L. Jiang, *Adv. Mater.*, 2015, **27**, 5010–5016.
88 P. Yin, T. Yao, Y. Wu, L. Zheng, Y. Lin, W. Liu, H. Ju, J. Zhu, X. Hong, Z. Deng, G. Zhou, S. Wei and Y. Li, *Angew. Chem., Int. Ed.*, 2016, **55**, 10800–10805.
89 X. Wang, Z. Chen, X. Zhao, T. Yao, W. Chen, R. You, C. Zhao, G. Wu, J. Wang, W. Huang, J. Yang, X. Hong, S. Wei, Y. Wu and Y. Li, *Angew. Chem., Int. Ed.*, 2018, **57**, 1944–1948.
90 X. Dai, Z. Chen, T. Yao, L. Zheng, Y. Lin, W. Liu, H. Ju, J. Zhu, X. Hong, S. Wei, Y. Wu and Y. Li, *Chem. Commun.*, 2017, **53**, 11568–11571.
91 Z. Li, Y. Chen, X. Lu, H. Li, L. Leng, T. Zhang and J. H. Horton, *Nano Res.*, 2022, **15**, 4023–4031.
92 S. Yuan, Z. Pu, H. Zhou, J. Yu, I. S. Amiinu, J. Zhu, Q. Liang, J. Yang, D. He, Z. Hu, G. Van Tendeloo and S. Mu, *Nano Energy*, 2019, **59**, 472–480.
93 L. Jiao, J. Zhu, Y. Zhang, W. Yang, S. Zhou, A. Li, C. Xie, X. Zheng, W. Zhou, S.-H. Yu and H.-L. Jiang, *J. Am. Chem. Soc.*, 2021, **143**, 19417–19424.
94 M. Xiao, J. Zhu, L. Ma, Z. Jin, J. Ge, X. Deng, Y. Hou, Q. He, J. Li, Q. Jia, S. Mukerjee, R. Yang, Z. Jiang, D. S. Su, C. Liu and W. Xing, *ACS Catal.*, 2018, **8**, 2824–2832.
95 G. Li, Y. Liu, Q. Zhang, Q. Hu, W. Guo, X. Cao, Y. Dou, L. Cheng, Y. Song, J. Su, L. Huang and R. Ye, *J. Mater. Chem. A*, 2022, **10**, 19254–19277.
96 J. Zhang, W. Cai, F. X. Hu, H. Yang and B. Liu, *Chem. Sci.*, 2021, **12**, 6800–6819.
97 Y. J. Sa, C. W. Lee, S. Y. Lee, J. Na, U. Lee and Y. J. Hwang, *Chem. Soc. Rev.*, 2020, **49**, 6632–6665.
98 T. K. Todorova, M. W. Schreiber and M. Fontecave, *ACS Catal.*, 2020, **10**, 1754–1768.
99 M. Li, H. Wang, W. Luo, P. C. Sherrell, J. Chen and J. Yang, *Adv. Mater.*, 2020, **32**, 2001848.
100 D. Gao, H. Zhou, F. Cai, J. Wang, G. Wang and X. Bao, *ACS Catal.*, 2018, **8**, 1510–1519.
101 C. Yang, Y. Wang, L. Qian, A. M. Al-Enizi, L. Zhang and G. Zheng, *ACS Appl. Energy Mater.*, 2021, **4**, 1034–1044.
102 W. Wang, S. Wang, X. Ma and J. Gong, *Chem. Soc. Rev.*, 2011, **40**, 3703–3727.
103 K. Fan, Y. Jia, Y. Ji, P. Kuang, B. Zhu, X. Liu and J. Yu, *ACS Catal.*, 2020, **10**, 358–364.
104 C. Ding, A. Li, S.-M. Lu, H. Zhang and C. Li, *ACS Catal.*, 2016, **6**, 6438–6443.
105 X.-M. Hu, H. H. Hval, E. T. Bjerglund, K. J. Dalgaard, M. R. Madsen, M.-M. Pohl, E. Welter, P. Lamagni, K. B. Buhl, M. Bremholm, M. Beller, S. U. Pedersen, T. Skrydstrup and K. Daasbjerg, *ACS Catal.*, 2018, **8**, 6255–6264.
106 P. Hou, W. Song, X. Wang, Z. Hu and P. Kang, *Small*, 2020, **16**, 2001896.
107 T. Liu, G. Wang and X. Bao, *J. Phys. Chem. C*, 2021, **125**, 26013–26020.
108 M. D. Hossain, Y. Huang, T. H. Yu, W. A. Goddard Iii and Z. Luo, *Nat. Commun.*, 2020, **11**, 2256.
109 S. Chen, X. Li, C.-W. Kao, T. Luo, K. Chen, J. Fu, C. Ma, H. Li, M. Li, T.-S. Chan and M. Liu, *Angew. Chem., Int. Ed.*, 2022, **61**, e202206233.
110 Z. Zhang and D. Wang, *J. Mater. Chem. A*, 2022, **10**, 5863–5877.
111 S. Liu, H. B. Yang, S.-F. Hung, J. Ding, W. Cai, L. Liu, J. Gao, X. Li, X. Ren, Z. Kuang, Y. Huang, T. Zhang and B. Liu, *Angew. Chem., Int. Ed.*, 2020, **59**, 798–803.
112 Y. Li, Y. Yan, Y. He and S. Du, *ACS Appl. Mater. Interfaces*, 2022, **14**, 11457–11464.
113 Z. Ma, U. Legrand, E. Pahija, J. R. Tavares and D. C. Boffito, *Ind. Eng. Chem. Res.*, 2021, **60**, 803–815.

Open Access Article. Published on 30 de novembre 2022. Downloaded on 27/1/2026 21:08:31.
This article is licensed under a Creative Commons Attribution 3.0 Unported Licence.

114 P. Bumroongsakulsawat and G. H. Kelsall, *Electrochim. Acta*, 2014, **141**, 216–225.
115 X. Yu and P. G. Pickup, *J. Power Sources*, 2008, **182**, 124–132.
116 M. Grasemann and G. Laurenczy, *Energy Environ. Sci.*, 2012, **5**, 8171–8181.
117 S. Back, J.-H. Kim, Y.-T. Kim and Y. Jung, *Phys. Chem. Chem. Phys.*, 2016, **18**, 9652–9657.
118 S. Zhao, S. Li, T. Guo, S. Zhang, J. Wang, Y. Wu and Y. Chen, *Nano-Micro Lett.*, 2019, **11**, 62.
119 Y.-X. Duan, Y.-T. Zhou, Z. Yu, D.-X. Liu, Z. Wen, J.-M. Yan and Q. Jiang, *Angew. Chem., Int. Ed.*, 2021, **60**, 8798–8802.
120 H. Wu, Z. Li, Y. Liu, X. Zou, L. Yin and S. Lin, *Sustain. Energy Fuels*, 2021, **5**, 5798–5803.
121 W.-B. Li, C. Yu, X.-Y. Tan, S. Cui, Y.-F. Zhang and J.-S. Qiu, *New Carbon Mater.*, 2022, **37**, 277–287.
122 P. Lu, X. Tan, H. Zhao, Q. Xiang, K. Liu, X. Zhao, X. Yin, X. Li, X. Hai, S. Xi, A. T. S. Wee, S. J. Pennycook, X. Yu, M. Yuan, J. Wu, G. Zhang, S. C. Smith and Z. Yin, *ACS Nano*, 2021, **15**, 5671–5678.
123 Y. Zhao, J. Liang, C. Wang, J. Ma and G. G. Wallace, *Adv. Energy Mater.*, 2018, **8**, 1702524.
124 T. Wang, J. Zhang, F. Li, B. Liu and S. Kawi, *Mater. Rep.: Energy*, 2022, **2**, 100140.
125 T. Tang, Z. Wang and J. Guan, *Adv. Funct. Mater.*, 2022, **32**, 2111504.
126 Z. Wang, J. Zhao and Q. Cai, *Phys. Chem. Chem. Phys.*, 2017, **19**, 23113–23121.
127 Y. Wu, Z. Jiang, X. Lu, Y. Liang and H. Wang, *Nature*, 2019, **575**, 639–642.
128 H. Yang, Y. Wu, G. Li, Q. Lin, Q. Hu, Q. Zhang, J. Liu and C. He, *J. Am. Chem. Soc.*, 2019, **141**, 12717–12723.
129 A. Guan, Z. Chen, Y. Quan, C. Peng, Z. Wang, T.-K. Sham, C. Yang, Y. Ji, L. Qian, X. Xu and G. Zheng, *ACS Energy Lett.*, 2020, **5**, 1044–1053.
130 L. Han, S. Song, M. Liu, S. Yao, Z. Liang, H. Cheng, Z. Ren, W. Liu, R. Lin, G. Qi, X. Liu, Q. Wu, J. Luo and H. L. Xin, *J. Am. Chem. Soc.*, 2020, **142**, 12563–12567.
131 R. Liu and C. Streb, *Adv. Energy Mater.*, 2021, **11**, 2101120.
132 W. Xu, H. Tang, H. Gu, H. Xi, P. Wu, B. Liang, Q. Liu and W. Chen, *J. Mater. Chem. A*, 2022, **10**, 14732–14746.
133 F. Pan, H. Zhang, K. Liu, D. Cullen, K. More, M. Wang, Z. Feng, G. Wang, G. Wu and Y. Li, *ACS Catal.*, 2018, **8**, 3116–3122.
134 X. Yang, J. Cheng, X. Xuan, N. Liu and J. Liu, *ACS Sustainable Chem. Eng.*, 2020, **8**, 10536–10543.
135 X. Li, H. Rong, J. Zhang, D. Wang and Y. Li, *Nano Res.*, 2020, **13**, 1842–1855.
136 X. Liu, Y. Liu, W. Yang, X. Feng and B. Wang, *Chem. – Eur. J.*, 2022, **28**, e202201471.
137 W. I. Choi, B. C. Wood, E. Schwegler and T. Ogitsu, *Adv. Energy Mater.*, 2015, **5**, 1501423.
138 Y. Hou, Y.-L. Liang, P.-C. Shi, Y.-B. Huang and R. Cao, *Appl. Catal. B: Environ.*, 2020, **271**, 118929.
139 P. Lu, Y. Yang, J. Yao, M. Wang, S. Dipazir, M. Yuan, J. Zhang, X. Wang, Z. Xie and G. Zhang, *Appl. Catal. B: Environ.*, 2019, **241**, 113–119.
140 Z. Chen, X. Zhang, W. Liu, M. Jiao, K. Mou, X. Zhang and L. Liu, *Energy Environ. Sci.*, 2021, **14**, 2349–2356.
141 L. Jiao, W. Yang, G. Wan, R. Zhang, X. Zheng, H. Zhou, S.-H. Yu and H.-L. Jiang, *Angew. Chem., Int. Ed.*, 2020, **59**, 22408–22413.
142 H. Wang, G. Liu, C. Chen, W. Tu, Y. Lu, S. Wu, D. O'Hare and R. Xu, *ACS Sustainable Chem. Eng.*, 2021, **9**, 3792–3801.
143 F. Dvořák, M. Farnesi Camellone, A. Tovt, N.-D. Tran, F. R. Negreiros, M. Vorokhta, T. Skála, I. Matolínová, J. Mysliveček, V. Matolín and S. Fabris, *Nat. Commun.*, 2016, **7**, 10801.
144 Y. Wang, M. Wang, Z. Zhang, Q. Wang, Z. Jiang, M. Lucero, X. Zhang, X. Li, M. Gu, Z. Feng and Y. Liang, *ACS Catal.*, 2019, **9**, 6252–6261.
145 N. Mohd Adli, W. Shan, S. Hwang, W. Samarakoon, S. Karakalos, Y. Li, D. A. Cullen, D. Su, Z. Feng, G. Wang and G. Wu, *Angew. Chem., Int. Ed.*, 2021, **60**, 1022–1032.
146 Z. Geng, Y. Cao, W. Chen, X. Kong, Y. Liu, T. Yao and Y. Lin, *Appl. Catal. B: Environ.*, 2019, **240**, 234–240.
147 Y. Zhou, L. Zheng, D. Yang, H. Yang, Q. Lu, Q. Zhang, L. Gu and X. Wang, *Small Methods*, 2021, **5**, 2000991.
148 D. Karapinar, N. T. Huan, N. Ranjbar Sahraie, J. Li, D. Wakerley, N. Touati, S. Zanna, D. Taverna, L. H. Galvão Tizei, A. Zitolo, F. Jaouen, V. Mougel and M. Fontecave, *Angew. Chem., Int. Ed.*, 2019, **58**, 15098–15103.
149 H. Cheng, X. Wu, X. Li, X. Nie, S. Fan, M. Feng, Z. Fan, M. Tan, Y. Chen and G. He, *Chem. Eng. J.*, 2021, **407**, 126842.
150 W. Guo, X. Tan, J. Bi, L. Xu, D. Yang, C. Chen, Q. Zhu, J. Ma, A. Tayal, J. Ma, Y. Huang, X. Sun, S. Liu and B. Han, *J. Am. Chem. Soc.*, 2021, **143**, 6877–6885.
151 H. Shang, T. Wang, J. Pei, Z. Jiang, D. Zhou, Y. Wang, H. Li, J. Dong, Z. Zhuang, W. Chen, D. Wang, J. Zhang and Y. Li, *Angew. Chem., Int. Ed.*, 2020, **59**, 22465–22469.
152 H. Cheng, X. Wu, M. Feng, X. Li, G. Lei, Z. Fan, D. Pan, F. Cui and G. He, *ACS Catal.*, 2021, **11**, 12673–12681.
153 Y. Zhang, L. Jiao, W. Yang, C. Xie and H.-L. Jiang, *Angew. Chem., Int. Ed.*, 2021, **60**, 7607–7611.
154 X. Song, H. Zhang, Y. Yang, B. Zhang, M. Zuo, X. Cao, J. Sun, C. Lin, X. Li and Z. Jiang, *Adv. Sci.*, 2018, **5**, 1800177.
155 Y.-N. Gong, L. Jiao, Y. Qian, C.-Y. Pan, L. Zheng, X. Cai, B. Liu, S.-H. Yu and H.-L. Jiang, *Angew. Chem., Int. Ed.*, 2020, **59**, 2705–2709.
156 T. Wang, X. Sang, W. Zheng, B. Yang, S. Yao, C. Lei, Z. Li, Q. He, J. Lu, L. Lei, L. Dai and Y. Hou, *Adv. Mater.*, 2020, **32**, 2002430.
157 S. Chen, Y. Li, Z. Bu, F. Yang, J. Luo, Q. An, Z. Zeng, J. Wang and S. Deng, *J. Mater. Chem. A*, 2021, **9**, 1705–1712.
158 X. Xuan, J. Cheng, X. Yang and J. Zhou, *ACS Sustainable Chem. Eng.*, 2020, **8**, 1679–1686.
159 Y. Wang, Y. Liu, W. Liu, J. Wu, Q. Li, Q. Feng, Z. Chen, X. Xiong, D. Wang and Y. Lei, *Energy Environ. Sci.*, 2020, **13**, 4609–4624.
160 M. Ma and Q. Tang, *J. Mater. Chem. C*, 2022, **10**, 15948–15956.
161 Z. Chen, A. Huang, K. Yu, T. Cui, Z. Zhuang, S. Liu, J. Li, R. Tu, K. Sun, X. Tan, J. Zhang, D. Liu, Y. Zhang, P. Jiang,

© 2023 The Author(s). Published by the Royal Society of Chemistry

Open Access Article. Published on 30 de novembre 2022. Downloaded on 27/1/2026 21:08:31.
This article is licensed under a Creative Commons Attribution 3.0 Unported Licence.

Y. Pan, C. Chen, Q. Peng and Y. Li, *Energy Environ. Sci.*, 2021, **14**, 3430–3437.
162 X. Hu, S. Yao, L. Chen, X. Zhang, M. Jiao, Z. Lu and Z. Zhou, *J. Mater. Chem. A*, 2021, **9**, 23515–23521.
163 Y. Wu, C. Chen, X. Yan, X. Sun, Q. Zhu, P. Li, Y. Li, S. Liu, J. Ma, Y. Huang and B. Han, *Angew. Chem., Int. Ed.*, 2021, **60**, 20803–20810.
164 Z. Li, R. Wu, S. Xiao, Y. Yang, L. Lai, J. S. Chen and Y. Chen, *Chem. Eng. J.*, 2022, **430**, 132882.
165 J.-X. Peng, W. Yang, Z. Jia, L. Jiao and H.-L. Jiang, *Nano Res.*, 2022, **15**, 10063–10069.
166 L. Meng, E. Zhang, H. Peng, Y. Wang, D. Wang, H. Rong and J. Zhang, *ChemCatChem*, 2022, **14**, e202101801.
167 R. Li and D. Wang, *Adv. Energy Mater.*, 2022, **12**, 2103564.
168 Y. Li, W. Shan, M. J. Zachman, M. Wang, S. Hwang, H. Tabassum, J. Yang, X. Yang, S. Karakalos, Z. Feng, G. Wang and G. Wu, *Angew. Chem., Int. Ed.*, 2022, **61**, e202205632.
169 Y. Hua, B. Zhang, W. Hao and Z. Gao, *Cell Rep. Phys. Sci.*, 2022, **3**, 100703.
170 T. He, A. R. P. Santiago, Y. Kong, M. A. Ahsan, R. Luque, A. Du and H. Pan, *Small*, 2022, **18**, 2106091.
171 Z. Liang, L. Song, M. Sun, B. Huang and Y. Du, *Sci. Adv.*, 2021, **7**, eabl4915.
172 D. Wu, B. He, Y. Wang, P. Lv, D. Ma and Y. Jia, *J. Phys. D: Appl. Phys.*, 2022, **55**, 203001.
173 N. Zhang, X. Zhang, Y. Kang, C. Ye, R. Jin, H. Yan, R. Lin, J. Yang, Q. Xu, Y. Wang, Q. Zhang, L. Gu, L. Liu, W. Song, J. Liu, D. Wang and Y. Li, *Angew. Chem., Int. Ed.*, 2021, **60**, 13388–13393.
174 J. Zhao, J. Zhao, F. Li and Z. Chen, *J. Phys. Chem. C*, 2018, **122**, 19712–19721.
175 X. Zhao, K. Zhao, Y. Liu, Y. Su, S. Chen, H. Yu and X. Quan, *ACS Catal.*, 2022, **12**, 11412–11420.
176 P. He, H. Feng, S. Wang, H. Ding, Y. Liang, M. Ling and X. Zhang, *Mater. Adv.*, 2022, **3**, 4566–4577.
177 S. Li, A. Guan, C. Yang, C. Peng, X. Lv, Y. Ji, Y. Quan, Q. Wang, L. Zhang and G. Zheng, *ACS Mater. Lett.*, 2021, **3**, 1729–1737.
178 L. Lin, H. Li, C. Yan, H. Li, R. Si, M. Li, J. Xiao, G. Wang and X. Bao, *Adv. Mater.*, 2019, **31**, 1903470.
179 W. Xie, H. Li, G. Cui, J. Li, Y. Song, S. Li, X. Zhang, J. Y. Lee, M. Shao and M. Wei, *Angew. Chem., Int. Ed.*, 2021, **60**, 7382–7388.
180 L. Lin, T. Liu, J. Xiao, H. Li, P. Wei, D. Gao, B. Nan, R. Si, G. Wang and X. Bao, *Angew. Chem., Int. Ed.*, 2020, **59**, 22408–22413.
181 M. Botifoll, I. Pinto-Huguet and J. Arbiol, *Nanoscale Horiz.*, 2022, **7**, 1427–1477.
182 Z. Liang, J. Wang, P. Tang, W. Tang, L. Liu, M. Shakouri, X. Wang, J. Llorca, S. Zhao, M. Heggen, R. E. Dunin-Borkowski, A. Cabot, H. B. Wu and J. Arbiol, *Appl. Catal. B: Environ.*, 2022, **314**, 121451.
183 Z. Liang, T. Zhang, P. Cao, T. Yoshida, W. Tang, X. Wang, Y. Zuo, P. Tang, M. Heggen, R. E. Dunin-Borkowski, J. R. Morante, A. Cabot, M. Yamashita and J. Arbiol, *Chem. Eng. J.*, 2022, **442**, 136129.

© 2023 The Author(s). Published by the Royal Society of Chemistry